


The emergent field of high entropy oxides: Design, prospects, challenges, and opportunities for tailoring material properties

Cite as: APL Mater. 8, 040912 (2020); <https://doi.org/10.1063/5.0003149>

Submitted: 30 January 2020 . Accepted: 22 March 2020 . Published Online: 20 April 2020

Brianna L. Musicó , Dustin Gilbert , Thomas Zac Ward , Katharine Page , Easo George , Jiaqiang Yan , David Mandrus , and Veerle Keppens 

COLLECTIONS

 This paper was selected as Featured



View Online



Export Citation



CrossMark

ARTICLES YOU MAY BE INTERESTED IN

[Aspects of the synthesis of thin film superconducting infinite-layer nickelates](#)

APL Materials **8**, 041107 (2020); <https://doi.org/10.1063/5.0005103>

[New approaches for achieving more perfect transition metal oxide thin films](#)

APL Materials **8**, 040904 (2020); <https://doi.org/10.1063/5.0003268>

[Epitaxial growth of \$\text{CH}_3\text{NH}_3\text{PbI}_3\$ on rubrene single crystal](#)

APL Materials **8**, 041104 (2020); <https://doi.org/10.1063/1.5142307>

APL Materials *Excellence in Research Award*

LEARN MORE >>



The emergent field of high entropy oxides: Design, prospects, challenges, and opportunities for tailoring material properties

Cite as: APL Mater. 8, 040912 (2020); doi: 10.1063/5.0003149

Submitted: 30 January 2020 • Accepted: 22 March 2020 •

Published Online: 20 April 2020



Brianna L. Musicó,¹  Dustin Gilbert,¹  Thomas Zac Ward,²  Katharine Page,¹  Easo George,^{1,2}  Jiaqiang Yan,^{1,2}  David Mandrus,^{1,2}  and Veerle Keppens^{1,a)} 

AFFILIATIONS

¹Department of Materials Science and Engineering, University of Tennessee, Knoxville, Tennessee 37996-4545, USA

²Materials Science and Technology Division, Oak Ridge National Laboratory, Oak Ridge, Tennessee 37831, USA

^{a)}Author to whom correspondence should be addressed: vkeppens@utk.edu

ABSTRACT

A new class of ceramics, called entropy stabilized oxides, High Entropy Oxides (HEOs), multicomponent oxides, compositionally complex oxides, or polycation oxides, has generated considerable research interest since the first report in 2015. This multicomponent approach has created new opportunities for materials design and discovery. This Perspective will highlight some current research developments and possible applications while also providing an overview of the many successfully synthesized HEO systems to date. The polycation approach to composition development will be discussed along with a few case studies, challenges, and future possibilities afforded by this novel class of materials.

© 2020 Author(s). All article content, except where otherwise noted, is licensed under a Creative Commons Attribution (CC BY) license (<http://creativecommons.org/licenses/by/4.0/>). <https://doi.org/10.1063/5.0003149>

I. INTRODUCTION

“High entropy” has become a commonplace term in materials research ever since a new method of alloy design was proposed in 2004, relying on the combination of multiple elements in equimolar ratios.^{1,2} This was the start of a new research focus, called High Entropy Alloys (HEAs) that is still active and growing. HEAs attracted interest because of the possibility that a solid solution of five or more elements could be stabilized due to high mixing entropy. The exceptional mechanical properties achieved by the multicomponent approach have dominated HEA research in the field of structural materials.³ More recently, HEAs have expanded to include the studies of electronic, ionic, magnetic, thermal, and superconducting properties.^{4–6}

Reports on the unique properties achieved with HEAs motivated the exploration of compositional complexity as an approach to materials design.⁷ The field of multi-component materials was expanded in 2015 to include High Entropy Oxides (HEOs)⁸ and was followed by high entropy metal diborides,⁹ high entropy carbides,¹⁰ high entropy sulfides,¹¹ high entropy fluorides,¹² and high entropy

alumino silicides,¹³ as depicted in Fig. 1. Metal oxides are attractive for applications,¹⁴ and multicomponent design could expand the available compositional space, providing greater flexibility to meet the demands of today’s advanced materials. HEOs also show great promise for applications in energy storage and catalysis. The electrochemical applications of HEOs, including the high Li-ion conductivity and Li-storage capabilities of rock salt-HEOs for use in battery applications, have been previously reviewed,¹⁵ and will therefore not be discussed extensively here. This Perspective will focus on the emergence of compositionally complex oxide materials; it will survey published work and discuss possible applications of HEO materials with a focus on entropy and materials design as well as synthesis considerations, and identify new directions enabled by the HEO class of materials.

II. ENTROPY AND MATERIALS DESIGN

A. Entropy is not the whole story

Whether a certain reaction is possible or not depends on whether the free energy decreases or increases. At constant pressure,



FIG. 1. Timeline for the development of the different classes of compositionally complex materials.

the relevant free energy is the Gibbs free energy, G , and the change in free energy, ΔG , associated with the reaction is given by: $\Delta G = \Delta H - T\Delta S$, where ΔH and ΔS are the corresponding changes in enthalpy and entropy, and T is the reaction temperature. When pure elements are mixed together, the enthalpy change to be considered in the above expression depends on the particular reaction pathway chosen: for example, it would be the mixing enthalpy (ΔH_{mix}) if a solid solution forms or the formation enthalpy (ΔH_f) if the reaction produces a compound. The relevant entropy change is due to the increased number of ways in which the elements can be arranged on the lattice of an alloy (configurational entropy change, ΔS_{conf}) or from other contributions (e.g., vibrational and magnetic entropy). ΔH_{mix} can be negative (in solid solutions that show a tendency to order), zero (in ideal solid solutions), or positive (in solid solutions with a tendency to cluster). In contrast, ΔH_f is always negative and ΔS_{conf} is always positive. Among the several possible reactions, the one with the most negative free energy change will be the thermodynamically most favored. Thus, to evaluate whether a solid solution or intermetallic compound forms when pure elements are mixed at a given temperature, one needs to know the relative magnitudes of ΔH_{mix} , ΔH_f , and ΔS_{conf} . For given values of these quantities, the entropic term would become increasingly important as the temperature is increased, tending to stabilize solid solutions at high temperatures.

In HEAs, it was initially proposed that the increased ΔS_{conf} of near-equiatomic alloys with 5 or more elements may favor the formation of solid solution phases over competing intermetallic compounds.⁷ However, experiments showed that configurational entropy is generally not able to override the competing driving forces, such as enthalpy, which also contribute to the phase stability.¹⁶ For example, the equiatomic alloy CoCrFeMnNi is known to solidify as a single-phase solid solution.² Since the change in ideal configurational entropy (mixing entropy) of an equiatomic alloy is given by $R \ln n$, where R is the gas constant and n is the number of elements in the alloy, its value for the CoCrFeMnNi alloy is $1.61 R$. This value will not change when individual elements are replaced one at a time to produce new alloys as long as n does not change. Thus, it is $1.61 R$ also in CoCrFeMnCu (where Cu replaces Ni in the original alloy). Otto *et al.*¹⁶ showed that every new alloy thus created (CoCrFeMnCu, CoMoFeMnNi, TiCrFeMnNi, etc.) rather than being a single-phase solid solution, phase-separated

into multiple metallic and intermetallic phases after 3-day anneals at high temperatures. Therefore, although in the CoCrFeMnNi alloy, entropic effects were stronger than enthalpic effects (at sufficiently high temperatures), in the other derivative alloys, enthalpic effects won out (at comparable temperatures). Even in the CoCrFeMnNi alloy, at lower temperatures ($<800^\circ\text{C}$), the single-phase solid solution decomposes into multiple metallic and intermetallic phases,¹⁷ consistent with the decreasing influence of entropy with decreasing temperature.

Recent work by Rost *et al.*⁸ has demonstrated analogous behavior in oxide mixtures. When they mixed five binary oxides (MgO, CoO, CuO, NiO, and ZnO) in equimolar proportions and heated the mixture in the $850\text{--}900^\circ\text{C}$ temperature range, a single-phase quinary HEO, $(\text{Mg}_{0.2}\text{Co}_{0.2}\text{Cu}_{0.2}\text{Ni}_{0.2}\text{Zn}_{0.2})\text{O}$, with the rock salt structure was observed to form, which separated into a two-phase mixture (rock salt and tenorite) at lower temperatures. The phase transformation from single-phase to two-phase and back was reversible with temperature, similar to that observed in the CrMnFeCoNi alloy,¹⁸ indicative of the increased/decreased contribution of configurational entropy at high/low temperatures. The authors attributed the increased configurational entropy of the HEO to the random distribution of cations on the cation sublattice sites, which was confirmed by extended x-ray absorption fine structure. Nevertheless, the formation of a single-phase quinary HEO is fascinating because its individual components (binary oxides) do not show complete solid solubility with each other. They also have different crystal structures: MgO, NiO, and CoO have the rock salt structure, CuO has the tenorite structure, and ZnO has the wurtzite structure. This is reminiscent of the CrMnFeCoNi HEA in which Ni, Fe, and Co (the latter two only at elevated temperatures) have the face-centered cubic structure, Cr has the body-centered cubic structure, and Mn has the complex A12 crystal structure; yet when mixed together, the result is a single-phase solid solution with the face-centered cubic crystal structure. In both cases, the formation enthalpy of competing phases appears to be low enough that it can be overcome by configurational entropy at elevated temperatures. Additional work has been done on this rock salt to investigate the effect that the grain size has on controlling the phase spectrum behavior.¹⁹ As in the rock salt system, a reversible multi-to-single phase transition was observed in later HEO perovskite work on $(\text{Gd}_{0.2}\text{La}_{0.2}\text{Nd}_{0.2}\text{Sm}_{0.2}\text{Y}_{0.2})\text{MnO}_3$, indicating entropy stabilized

behavior along with information supporting that the 10-cationic system ($\text{Gd}_{0.2}\text{La}_{0.2}\text{Nd}_{0.2}\text{Sm}_{0.2}\text{Y}_{0.2}$) ($\text{Co}_{0.2}\text{Cr}_{0.2}\text{Fe}_{0.2}\text{Mn}_{0.2}\text{Ni}_{0.2}$) O_3 is also most likely entropy stabilized, extending the concept of entropy stabilization to multicomponent perovskites.²⁰ Work on a five-component fluorite ($\text{Ce}_{0.2}\text{Zr}_{0.2}\text{Hf}_{0.2}\text{Sn}_{0.2}\text{Ti}_{0.2}$) O_2 also showed a reversible multi-phase to single-phase transition, indicating entropy stabilization of the compound.²¹ An interesting aspect of the formation of these perovskites is the stabilization of the lower symmetry orthorhombic phase, whereas the rock salt⁸ and fluorite type²² had a preference to maintain a high symmetry structure, which suggests an enthalpy contribution to octahedral tilt Jahn–Teller type distortion, making an adaptation to the cubic phase energetically costly.²⁰ While the nominal work in this field showed the rock salt ($\text{Mg}_{0.2}\text{Ni}_{0.2}\text{Co}_{0.2}\text{Cu}_{0.2}\text{Zn}_{0.2}$) O composition to be truly entropy stabilized, this has not been verified for many of the other compositions in the literature. The recent review of the electrochemical applications of HEOs points out that entropy stabilization may be contributing to not just phase stability, but to the functional properties as well, as shown in the reversible de/lithiation behavior of the rock salt based HEOs.¹⁵ The differentiation between compositionally complex materials that are truly entropy stabilized vs multicomponent solid solutions is imperative as research in this area continues to progress.

There are also key differences that are worth noting. For example, in the rock salt HEO mentioned earlier, removal of *any one* of the components (binary oxides) from the quinary mixture to produce a quaternary mixture results in the loss of the single-phase rock salt structure and decomposition into multiphase structures.⁸ This is consistent with the notion that a decrease in the configurational entropy (quinary to quaternary) decreases the stability of the solid solution. In contrast, removal of several of the components (elements) from the quinary HEA CrMnFeCoNi (Mn, Cr, and Fe) to form quaternaries (FeNiCoCr, FeNiCoMn, and NiCoCrMn) retains the single-phase solid solution state.²³ The lower configurational entropy of the metallic quaternaries presumably is sufficient to overcome the enthalpy of competing intermetallic phases whereas that of the oxide quaternaries is insufficient to overcome the enthalpy of competing oxide phases. Another difference is that, in some perovskite, spinel, and fluorite HEOs, when certain cation species are switched out for others based on ionic

radii, not all compositions stabilize as a single phase.^{24,26} Additionally, rare-earth oxides crystallizing in the fluorite CaF_2 type structure with 5 elements on the rare-earth site form a single phase only with the addition of cerium, showing evidence of cerium as a stabilizer in this case.²² This is reminiscent of the HEA results¹⁶ discussed earlier.

Materials design is challenging given that entropy is but one factor contributing to the phase stability of ceramic compounds. In some cases, if the system's configurational entropy is large enough, it can be a stabilizing factor, as shown in the seminal HEO work.⁸ In general, though, the picture is much more complicated, and it is necessary to take into account variables, such as the charge states and the ionic radii of the individual cations. Understanding the underlying reasons behind compositional effects on phase stability and distinguishing entropy-stabilized material systems vs solid solutions is an important area for future investigation.

B. Selection criteria and synthesis

The initial work of Rost *et al.* showed that even in cases where (i) the component binary oxides do not exhibit uniform crystal structure, electronegativity, or cation coordination, and (ii) the pairs of binary oxides do not exhibit extensive mutual solubility, it may be possible to obtain single-phase solid solutions if the entire collection is isovalent.⁸ In later studies, the initial oxidation state of the starting materials has not proven to be a primary factor in the formation of the desired phase, as equilibrium can be reached at high temperatures with oxygen loss and preserved upon quenching.²⁷ This aliovalent substitution widens the possibilities for compositional variation and in turn properties and applications. The synthesis of $(\text{Co,Cr,Fe,Mn,Ni})_3\text{O}_4$ shows the expansion into other crystal structures with the creation of a single-phase HEO with either spinel or rock salt structure by means of varying the oxygen partial pressure.²⁸ This manipulation of the synthesis method was not something that was seen or able to be used in HEA systems, but should be considered with other oxide synthesis methods (see Table I) as the broader range of structures are available in oxides, as shown by the timeline in Fig. 2, which opens up possibilities to maximize the potential of this new class of materials.

TABLE I. Summary of high entropy oxide compounds synthesized in the literature, their crystal structure, synthesis method, their investigated properties/application, and reference. "ES" indicates that the study showed the composition to be entropy stabilized.

Crystal structure	Compound(s)	Synthesis	Investigated property or application	Reference
Rock salt (Fm-3m)	$(\text{Co}_{0.25}\text{Mg}_{0.25}\text{Ni}_{0.25}\text{Zn}_{0.25})\text{O}$ and $(\text{Co}_{0.2}\text{Cu}_{0.2}\text{Mg}_{0.2}\text{Ni}_{0.2}\text{Zn}_{0.2})\text{O}$	Nebulized spray pyrolysis, flame spray pyrolysis, reverse co-precipitation	Synthesis method for phase stability	66
Rock salt (Fm-3m)	$(\text{Mg}_{0.25(1-x)}\text{Co}_x\text{Cu}_{0.25(1-x)}\text{Ni}_{0.25(1-x)}\text{Zn}_{0.25(1-x)})\text{O}$, $x = 0.2, 0.27, \text{ and } 0.33$	Pulsed laser deposition	Exchange bias	58
Rock salt (Fm-3m)	$(\text{Mg}_{0.2}\text{Co}_{0.2}\text{Cu}_{0.2}\text{Ni}_{0.2}\text{Zn}_{0.2})\text{O}$, ES	Solid state synthesis	Entropy stabilization local structure	8 and 42

TABLE I. (Continued.)

Crystal structure	Compound(s)	Synthesis	Investigated property or application	Reference
Rock salt (Fm-3m)	$(\text{Mg}_{0.2}\text{Co}_{0.2}\text{Cu}_{0.2}\text{Ni}_{0.2}\text{Zn}_{0.2})_{1-x}\text{Li}_x\text{O}$, $(\text{Mg}_{0.2}\text{Co}_{0.2}\text{Cu}_{0.2}\text{Ni}_{0.2}\text{Zn}_{0.2})_{1-2x}(\text{LiGa})_x\text{O}$, $(\text{Mg}_{0.2}\text{Co}_{0.2}\text{Cu}_{0.2}\text{Ni}_{0.2}\text{Zn}_{0.2})_{0.8}(\text{LiGa})_{0.2}\text{O}$, $(\text{Mg}_{0.2}\text{Co}_{0.2}\text{Cu}_{0.2}\text{Ni}_{0.2}\text{Zn}_{0.2})_{1-x}\text{Li}_x\text{O}$, $(\text{Mg}_{0.2}\text{Co}_{0.2}\text{Cu}_{0.2}\text{Ni}_{0.2}\text{Zn}_{0.2})_{1-x}\text{Na}_x\text{O}$, and $(\text{Mg}_{0.2}\text{Co}_{0.2}\text{Cu}_{0.2}\text{Ni}_{0.2}\text{Zn}_{0.2})_{0.95}\text{K}_{0.05}\text{O}$	Solid state synthesis	Dielectric properties	27 and 67
Rock salt (Fm-3m)	$(\text{Mg}_{0.2}\text{Co}_{0.2}\text{Cu}_{0.2}\text{Ni}_{0.2}\text{Zn}_{0.2})\text{O}$, $(\text{Mg}_{0.25}\text{Co}_{0.25}\text{Cu}_{0.25}\text{Ni}_{0.25})\text{O}$, $(\text{Mg}_{0.25}\text{Co}_{0.25}\text{Ni}_{0.25}\text{Zn}_{0.25})\text{O}$, and $(\text{Mg}_{0.25}\text{Cu}_{0.25}\text{Ni}_{0.25}\text{Zn}_{0.25})\text{O}$	Nebulized spray pyrolysis	Reversible energy storage	68
Rock salt (Fm-3m)	$(\text{Mg}_{0.2}\text{Co}_{0.2}\text{Cu}_{0.2}\text{Ni}_{0.2}\text{Zn}_{0.2})\text{O}$, and PtMgCoCuNiZnO (0.3 wt% Pt)	Physical mixture and co-precipitation	Catalysts with high-temperature stabilities	69
Rock salt (Fm-3m)	$(\text{MgCoNiZn})_{1-x}\text{Cu}_x\text{O}$ ($x = 0.13, 0.2$, and 0.26)	N/A DFT studies	First-principles study	43
Rock salt (Fm-3m)	$(\text{Mg}_{0.2}\text{Co}_{0.2}\text{Cu}_{0.2}\text{Ni}_{0.2}\text{Zn}_{0.2})\text{O}$	Co-precipitation and hydrothermal synthesis	Density	70
Rock salt (Fm-3m)	$(\text{Mg}_{0.2}\text{Co}_{0.2}\text{Cu}_{0.2}\text{Ni}_{0.2}\text{Zn}_{0.2})\text{O}$, $(\text{Mg}_x\text{Co}_x\text{Cu}_x\text{Ni}_x\text{Zn}_x\text{Sc}_x)\text{O}$ ($x \sim 0.167$), and $(\text{Mg}_x\text{Co}_x\text{Cu}_x\text{Ni}_x\text{Zn}_x\text{Li}_x)\text{O}$ ($x \sim 0.167$)	Solid state synthesis, pulsed laser deposition, DFT studies	DFT studies of lattice stability	71
Rock salt (Fm-3m)	$(\text{Mg}_{0.2}\text{Co}_{0.2}\text{Cu}_{0.2}\text{Ni}_{0.2}\text{Zn}_{0.2})\text{O}$	Solid state synthesis	Diffraction study of Jahn–Teller distortion	40
Rock salt (Fm-3m)	$(\text{Mg}_x\text{Co}_x\text{Cu}_x\text{Ni}_x\text{Zn}_x\text{Sc}_x)\text{O}$ ($x \sim 0.167$)	Pulsed laser deposition	Different growth conditions to modulate particle kinetic energy and plume reactivity	72
Rock salt (Fm-3m)	$\text{Mg}_x\text{Ni}_x\text{Cu}_x\text{Co}_x\text{Zn}_x\text{O}$ ($x = 0.2$), $\text{Mg}_x\text{Ni}_x\text{Cu}_x\text{Co}_x\text{Zn}_x\text{Sc}_x\text{O}$ ($x = 0.167$), $\text{Mg}_x\text{Ni}_x\text{Cu}_x\text{Co}_x\text{Zn}_x\text{Sb}_x\text{O}$ ($x = 0.167$), $\text{Mg}_x\text{Ni}_x\text{Cu}_x\text{Co}_x\text{Zn}_x\text{Sn}_x\text{O}$ ($x = 0.167$), $\text{Mg}_x\text{Ni}_x\text{Cu}_x\text{Co}_x\text{Zn}_x\text{Cr}_x\text{O}$ ($x = 0.167$), and $\text{Mg}_x\text{Ni}_x\text{Cu}_x\text{Co}_x\text{Zn}_x\text{Ge}_x\text{O}$ ($x = 0.167$)	Pulsed laser deposition	Charge induced disorder controlled thermal conductivity	47
Rock salt (Fm-3m)	$(\text{Mg}_{0.2}\text{Co}_{0.2}\text{Cu}_{0.2}\text{Ni}_{0.2}\text{Zn}_{0.2})\text{O}$	Solid state synthesis	Reaction sequence and mechanical properties	60
Rock salt (Fm-3m)	$(\text{Co}_{0.2}\text{Cu}_{0.2}\text{Mg}_{0.2}\text{Ni}_{0.2}\text{Zn}_{0.2})\text{O}$ electrode material in full-cells with a $\text{LiNi}_{1/3}\text{Co}_{1/3}\text{Mn}_{1/3}\text{O}_2$ cathode	Nebulized spray pyrolysis	Lithium ion battery applications	73
Rock salt (Fm-3m)	$(\text{Mg}_{0.2}\text{Co}_{0.2}\text{Cu}_{0.2}\text{Ni}_{0.2}\text{Zn}_{0.2})\text{O}$	Solid state synthesis	Anode material for lithium ion batteries	74
Rock salt (Fm-3m)	$(\text{Mg}_{0.2}\text{Co}_{0.2}\text{Ni}_{0.2}\text{Cu}_{0.2}\text{Zn}_{0.2})\text{O}$, $(\text{Co}_{0.2}\text{Ni}_{0.2}\text{Cu}_{0.2}\text{Zn}_{0.2}\text{Li}_{0.1}\text{Ga}_{0.1})\text{O}$, $(\text{Mg}_{0.2}\text{Co}_{0.2}\text{Ni}_{0.2}\text{Cu}_{0.2}\text{Li}_{0.1}\text{Ga}_{0.1})\text{O}$, $(\text{Mg}_{0.19}\text{Co}_{0.19}\text{Ni}_{0.19}\text{Cu}_{0.19}\text{Zn}_{0.19}\text{Li}_{0.05})\text{O}$, $(\text{Mg}_{0.2}\text{Ni}_{0.2}\text{Cu}_{0.2}\text{Zn}_{0.2}\text{Li}_{0.1}\text{Ga}_{0.1})\text{O}$, $(\text{Mg}_{0.2}\text{Co}_{0.2}\text{Cu}_{0.2}\text{Zn}_{0.2}\text{Li}_{0.1}\text{Ga}_{0.1})\text{O}$, $(\text{Mg}_{0.2}\text{Co}_{0.2}\text{Ni}_{0.2}\text{Zn}_{0.2}\text{Li}_{0.1}\text{Ga}_{0.1})\text{O}$, and $(\text{Mg}_{0.16}\text{Co}_{0.16}\text{Ni}_{0.16}\text{Cu}_{0.16}\text{Zn}_{0.16}\text{Li}_{0.10}\text{Fe}_{0.10})\text{O}$	Solid state synthesis	Influence of substitution on magnetic properties	32

TABLE I. (Continued.)

Crystal structure	Compound(s)	Synthesis	Investigated property or application	Reference
Rock salt (Fm-3m)	$(\text{Mg}_{0.2}\text{Co}_{0.2}\text{Cu}_{0.2}\text{Ni}_{0.2}\text{Zn}_{0.2})\text{O}$	Solid state synthesis	Neutron diffraction, magnetic structure and properties	33
Rock salt: Fm-3m, fluorite: Fm-3m, perovskite: Pbm̄n	$(\text{Co}_{0.2}\text{Cu}_{0.2}\text{Mg}_{0.2}\text{Ni}_{0.2}\text{Zn}_{0.2})\text{O}$, $(\text{Ce}_{0.2}\text{La}_{0.2}\text{Pr}_{0.2}\text{Sm}_{0.2}\text{Y}_{0.2})\text{O}_{2-\delta}$, $(\text{Gd}_{0.2}\text{La}_{0.2}\text{Nd}_{0.2}\text{Sm}_{0.2}\text{Y}_{0.2})$ $(\text{Co}_{0.2}\text{Cr}_{0.2}\text{Mn}_{0.2}\text{Fe}_{0.2}\text{Ni}_{0.2})\text{O}_3$	Nebulized spray pyrolysis	Homogeneity at the atomic scale	30
Rock salt (Fm-3m)	$(\text{Al}_{0.31}\text{Cr}_{0.20}\text{Fe}_{0.14}\text{Ni}_{0.35})\text{O}$	Radio frequency (RF) reactive magnetron sputtering	Effects of helium implantation on mechanical properties	75
Rock salt (Fm-3m)	$(\text{MgCoNiCuZn})_{1-x}\text{Li}_x\text{O}$ ($x = 0-0.3$)	Solid state synthesis	Charge compensation mechanisms	76
Rock salt (Fm-3m)	$(\text{Li}_x(\text{Co}_{0.2}\text{Cu}_{0.2}\text{Mg}_{0.2}\text{Ni}_{0.2}\text{Zn}_{0.2})\text{OF}_x)$ and $\text{Na}_y(\text{Co}_{0.2}\text{Cu}_{0.2}\text{Mg}_{0.2}\text{Ni}_{0.2}\text{Zn}_{0.2})\text{OCl}_y$	Solid state synthesis	Energy storage: Enhanced Li storage properties	36
Rock salt (Fm-3m)	$(\text{NiMgCuZnCo})\text{O}$ and 2 and 5 wt. % $\text{Pt/Ru}-(\text{NiMgCuZnCo})\text{O}$	Mechano-chemical synthesis	High temperature stability catalytic ability	39
Rock salt (Fm-3m)	Li/Mn doped $(\text{Mg}_{0.2}\text{Co}_{0.2}\text{Cu}_{0.2}\text{Ni}_{0.2}\text{Zn}_{0.2})\text{O}$	Solid state synthesis	Thermal and compressive stability at high temperatures	77
Rock salt (Fm-3m)	$(\text{Mg}_{0.2}\text{Co}_{0.2}\text{Cu}_{0.2}\text{Ni}_{0.2}\text{Zn}_{0.2})\text{O}$, ES	Solid state synthesis with conventional sintering and spark plasma sintering	Study of the effect of grain size on controlling the volume fractions of a secondary phase and entropic single-phase	19
Spinel-rock salt two-phase oxide system	$(\text{FeMgCoNi})\text{O}_x$	Solid state synthesis	Thermochemical water splitting at low temperatures	78
Mesoporous structure and single rock salt phase	$(\text{CuNiFeCoMg})\text{O}_x\text{-Al}_2\text{O}_3$	Mechanochemical nonhydrolytic sol–gel method	Mesoporous high entropy metal oxide synthesis and superior SO_2 -resisting performance in the catalytic oxidation of CO	79
Rock salt (Fm-3m)	$(\text{Mg}_{0.2}\text{Co}_{0.2}\text{Cu}_{0.2}\text{Ni}_{0.2}\text{Zn}_{0.2})\text{O}$	Mechanochemical synthesis	Microstructure and electrical conductivity with temperature	80
Rock salt (Fm-3m)	$(\text{Mg}_{0.2}\text{Co}_{0.2}\text{Ni}_{0.2}\text{Cu}_{0.2}\text{Zn}_{0.2})\text{O}$	Solid state synthesis and laser molecular beam epitaxy	Tunable pseudocapacitive contribution to achieve superior lithium-storage properties	81
Rock salt (Fm-3m)	$(\text{Mg}_{0.25(1-x)}\text{Co}_{0.25(1-x)}\text{Ni}_{0.25(1-x)}\text{Cu}_x\text{Zn}_{0.25(1-x)})\text{O}$ ($x = 0.11, 0.17, 0.20, 0.24$, and 0.27) and $(\text{Mg}_{0.25(1-x)}\text{Co}_x\text{Ni}_{0.25(1-x)}\text{Cu}_{0.25(1-x)}\text{Zn}_{0.25(1-x)})\text{O}$ ($x = 0.20, 0.27$, and 0.33)	Epitaxial films	Magnetic frustration control through tunable stereochemically driven disorder	38

TABLE I. (Continued.)

Crystal structure	Compound(s)	Synthesis	Investigated property or application	Reference
Rock salt (Fm-3m)	$(\text{Mg}_{0.2}\text{Co}_{0.2}\text{Ni}_{0.2}\text{Cu}_{0.2}\text{Zn}_{0.2})\text{O}$	Comparison of experimental values from Ref. 47 with molecular dynamics values and Bridgman equation	Influence of mass and charge disorder on the phonon thermal conductivity of entropy stabilized oxides determined by molecular dynamics simulations	50
Orthorhombic perovskite (Pbnm)	$(\text{Gd}_{0.2}\text{La}_{0.2}\text{Nd}_{0.2}\text{Sm}_{0.2}\text{Y}_{0.2})\text{MnO}_3$, ES, $(\text{Gd}_{0.2}\text{La}_{0.2}\text{Nd}_{0.2}\text{Sm}_{0.2}\text{Y}_{0.2})\text{FeO}_3$, $(\text{Gd}_{0.2}\text{La}_{0.2}\text{Nd}_{0.2}\text{Sm}_{0.2}\text{Y}_{0.2})\text{CrO}_3$, $(\text{Gd}_{0.2}\text{La}_{0.2}\text{Nd}_{0.2}\text{Sm}_{0.2}\text{Y}_{0.2})\text{CoO}_3$, $\text{Y}(\text{Co}_{0.2}\text{Cr}_{0.2}\text{Fe}_{0.2}\text{Mn}_{0.2}\text{Ni}_{0.2})\text{O}_3$, $\text{Sm}(\text{Co}_{0.2}\text{Cr}_{0.2}\text{Fe}_{0.2}\text{Mn}_{0.2}\text{Ni}_{0.2})\text{O}_3$, $\text{Nd}(\text{Co}_{0.2}\text{Cr}_{0.2}\text{Fe}_{0.2}\text{Mn}_{0.2}\text{Ni}_{0.2})\text{O}_3$, $\text{La}(\text{Co}_{0.2}\text{Cr}_{0.2}\text{Fe}_{0.2}\text{Mn}_{0.2}\text{Ni}_{0.2})\text{O}_3$, $\text{Gd}(\text{Co}_{0.2}\text{Cr}_{0.2}\text{Fe}_{0.2}\text{Mn}_{0.2}\text{Ni}_{0.2})\text{O}_3$, and $(\text{Gd}_{0.2}\text{La}_{0.2}\text{Nd}_{0.2}\text{Sm}_{0.2}\text{Y}_{0.2})(\text{Co}_{0.2}\text{Cr}_{0.2}\text{Fe}_{0.2}\text{Mn}_{0.2}\text{Ni}_{0.2})\text{O}_3$	Nebulized spray pyrolysis	Synthesis and phase stability with HTXRD	20
Orthorhombic perovskite (Pbnm)	$\text{Gd}(\text{Co}_{0.2}\text{Cr}_{0.2}\text{Fe}_{0.2}\text{Mn}_{0.2}\text{Ni}_{0.2})\text{O}_3$, $\text{La}(\text{Co}_{0.2}\text{Cr}_{0.2}\text{Fe}_{0.2}\text{Mn}_{0.2}\text{Ni}_{0.2})\text{O}_3$, $\text{Nd}(\text{Co}_{0.2}\text{Cr}_{0.2}\text{Fe}_{0.2}\text{Mn}_{0.2}\text{Ni}_{0.2})\text{O}_3$, $\text{Sm}(\text{Co}_{0.2}\text{Cr}_{0.2}\text{Fe}_{0.2}\text{Mn}_{0.2}\text{Ni}_{0.2})\text{O}_3$, $\text{Y}(\text{Co}_{0.2}\text{Cr}_{0.2}\text{Fe}_{0.2}\text{Mn}_{0.2}\text{Ni}_{0.2})\text{O}_3$, and $(\text{Gd}_{0.2}\text{La}_{0.2}\text{Nd}_{0.2}\text{Sm}_{0.2}\text{Y}_{0.2})(\text{Co}_{0.2}\text{Cr}_{0.2}\text{Fe}_{0.2}\text{Mn}_{0.2}\text{Ni}_{0.2})\text{O}_3$	Nebulized spray pyrolysis	Magnetic and Mössbauer characterization	41
Orthorhombic perovskite (Pbnm)	$\text{La}(\text{Cr}_{0.2}\text{Mn}_{0.2}\text{Fe}_{0.2}\text{Co}_{0.2}\text{Ni}_{0.2})\text{O}_3$	Solid-state synthesis and pulsed laser epitaxy	Strain mismatch, microstructure, atomic resolution, and magnetic properties showing anisotropy	55
Perovskite cubic (Pm-3m)	$\text{Sr}(\text{Zr}_{0.2}\text{Sn}_{0.2}\text{Ti}_{0.2}\text{Hf}_{0.2}\text{Mn}_{0.2})\text{O}_3$, $\text{Sr}(\text{Zr}_{0.2}\text{Sn}_{0.2}\text{Ti}_{0.2}\text{Hf}_{0.2}\text{Nb}_{0.2})\text{O}_3$, $\text{Ba}(\text{Zr}_{0.2}\text{Sn}_{0.2}\text{Ti}_{0.2}\text{Hf}_{0.2}\text{Ce}_{0.2})\text{O}_3$, $\text{Ba}(\text{Zr}_{0.2}\text{Sn}_{0.2}\text{Ti}_{0.2}\text{Hf}_{0.2}\text{Y}_{0.2})\text{O}_{3-x}$, $\text{Ba}(\text{Zr}_{0.2}\text{Sn}_{0.2}\text{Ti}_{0.2}\text{Hf}_{0.2}\text{Nb}_{0.2})\text{O}_3$, and $(\text{Sr}_{0.5}\text{Ba}_{0.5})(\text{Zr}_{0.2}\text{Sn}_{0.2}\text{Ti}_{0.2}\text{Hf}_{0.2}\text{Nb}_{0.2})\text{O}_3$	Solid state synthesis	Phase formation and stability	25
Perovskite cubic (Pm-3m)	$\text{Ba}(\text{Zr}_{0.2}\text{Sn}_{0.2}\text{Ti}_{0.2}\text{Hf}_{0.2}\text{Nb}_{0.2})\text{O}_3$	Pulsed laser deposition	Thermal conductivity	34
Perovskite cubic (Pm-3m)	$\text{Sr}((\text{Zr}_{0.94}\text{Y}_{0.06})_{0.2}\text{Sn}_{0.2}\text{Ti}_{0.2}\text{Hf}_{0.2}\text{Mn}_{0.2})\text{O}_{3-x}$	Spark plasma sintering	Density	82
Perovskite cubic (Pm-3m)	$\text{Ba}_{0.5}\text{Sr}_{0.5}(\text{Zr}_{0.4}\text{Hf}_{0.3}\text{Ti}_{0.3})\text{O}_3$, $\text{Ba}_{0.4}\text{Sr}_{0.4}\text{Bi}_{0.2}(\text{Zr}_{0.3}\text{Hf}_{0.3}\text{Ti}_{0.2}\text{Fe}_{0.2})\text{O}_3$, and $\text{Ru}_{0.13}/\text{Ba}_{0.3}\text{Sr}_{0.3}\text{Bi}_{0.4}(\text{Zr}_{0.2}\text{Hf}_{0.2}\text{Ti}_{0.2}\text{Fe}_{0.27})\text{O}_3$	Sonochemical-based method	Nanoparticles with good catalytic activity for CO	35
Orthorhombic perovskite (Pbnm)	$(\text{La}_{0.2}\text{Pr}_{0.2}\text{Nd}_{0.2}\text{Sm}_{0.2}\text{Eu}_{0.2})\text{NiO}_3$	Pulsed laser deposition	Valence state, temperature dependent electrical transport measurements	83

TABLE I. (Continued.)

Crystal structure	Compound(s)	Synthesis	Investigated property or application	Reference
Perovskite, cubic (Pm-3m)	$\text{Ba}(\text{Zr}_{0.2}\text{Ti}_{0.2}\text{Sn}_{0.2}\text{Hf}_{0.2}\text{Me}_{0.2})\text{O}_3$ (Me = Y^{3+} , Nb^{5+} , Ta^{5+} , V^{5+} , Mo^{6+} , and W^{6+})	Solid state synthesis	Microstructure and dielectric properties	84
Perovskite cubic (Pm-3m)	$(\text{Na}_{0.2}\text{Bi}_{0.2}\text{Ba}_{0.2}\text{Sr}_{0.2}\text{Ca}_{0.2})\text{TiO}_3$	Solid state synthesis	Dielectric properties and electrocaloric effect	85
Cubic-Bixbyite	$(\text{Gd}_{0.4}\text{Tb}_{0.4}\text{Dy}_{0.4}\text{Ho}_{0.4}\text{Er}_{0.4})\text{O}_3$	Polymeric steric entrapment	Synthesis and high temperature phase stability	31
Fluorite (Fm-3m)	$(\text{Hf}_{0.25}\text{Zr}_{0.25}\text{Ce}_{0.25})(\text{Y}_{0.25})\text{O}_{2-x}$, $(\text{Hf}_{0.25}\text{Zr}_{0.25}\text{Ce}_{0.25})(\text{Y}_{0.125}\text{Yb}_{0.125})\text{O}_{2-x}$, $(\text{Hf}_{0.2}\text{Zr}_{0.2}\text{Ce}_{0.2})(\text{Y}_{0.2}\text{Yb}_{0.2})\text{O}_{2-x}$, $(\text{Hf}_{0.25}\text{Zr}_{0.25}\text{Ce}_{0.25})(\text{Y}_{0.125}\text{Ca}_{0.125})\text{O}_{2-x}$, $(\text{Hf}_{0.25}\text{Zr}_{0.25}\text{Ce}_{0.25})(\text{Y}_{0.125}\text{Gd}_{0.125})\text{O}_{2-x}$, $(\text{Hf}_{0.2}\text{Zr}_{0.2}\text{Ce}_{0.2})(\text{Y}_{0.2}\text{Gd}_{0.2})\text{O}_{2-x}$, $(\text{Hf}_{0.25}\text{Zr}_{0.25}\text{Ce}_{0.25})(\text{Yb}_{0.125}\text{Gd}_{0.125})\text{O}_{2-x}$, and $(\text{Hf}_{0.2}\text{Zr}_{0.2}\text{Ce}_{0.2})(\text{Yb}_{0.2}\text{Gd}_{0.2})\text{O}_{2-x}$	Ball mill, spark plasma sintering, and annealing	Lower thermal conductivities	86
Fluorite (Fm-3m), Bixbyite (Ia-3)	$(\text{Ce},\text{Gd},\text{La},\text{Nd},\text{Pr},\text{Sm},\text{Y})\text{O}_{2-\delta}$, $(\text{Ce},\text{La},\text{Nd},\text{Pr},\text{Sm},\text{Y})\text{O}_{2-\delta}$, $(\text{Ce},\text{La},\text{Pr},\text{Sm},\text{Y})\text{O}_{2-\delta}$, $(\text{Ce},\text{La},\text{Pr},\text{Y})\text{O}_{2-\delta}$, $(\text{Ce},\text{La},\text{Pr},\text{Sm})\text{O}_{2-\delta}$, $(\text{Ce},\text{La},\text{Pr})\text{O}_{2-\delta}$, $(\text{Ce},\text{Pr})\text{O}_{2-\delta}$, $(\text{Ce},\text{Gd},\text{La},\text{Nd},\text{Pr},\text{Sm},\text{Y})\text{O}_{2-\delta}$, $(\text{Ce},\text{La},\text{Nd},\text{Pr},\text{Sm},\text{Y})\text{O}_{2-\delta}$, and $(\text{Ce},\text{La},\text{Pr},\text{Sm},\text{Y})\text{O}_{2-\delta}$	Nebulized spray pyrolysis (NSP), post-NSP, and calcination	Optical properties	29
Fluorite (Fm-3m)	$(\text{Ce}_{0.2}\text{Zr}_{0.2}\text{Hf}_{0.2}\text{Sn}_{0.2}\text{Ti}_{0.2})\text{O}_2$, ES	Solid state synthesis	Thermal conductivity and entropy stabilization	21
Fluorite (Fm-3m)	$(\text{Sc}_{0.2}\text{Ce}_{0.2}\text{Pr}_{0.2}\text{Gd}_{0.2}\text{Ho}_{0.2})_2\text{O}_{3\pm\delta}$	Precipitation	Synthesis, structure, and surface morphology of HEO nanoparticles	87
Fluorite (Fm-3m)	$(\text{Gd}_{0.2}\text{La}_{0.2}\text{Y}_{0.2}\text{Hf}_{0.2}\text{Zr}_{0.2})\text{O}_2$ $(\text{Gd}_{0.2}\text{La}_{0.2}\text{Ce}_{0.2}\text{Hf}_{0.2}\text{Zr}_{0.2})\text{O}_2$	Chemical co-precipitation followed by peptization in acidic medium under mild conditions	Confirmation of synthesis of single-phase nanoparticles	88
Fluorite (Fm-3m)	$(\text{Ce}_{0.2}\text{La}_{0.2}\text{Pr}_{0.2}\text{Sm}_{0.2}\text{Y}_{0.2})\text{O}_{2-\delta}$	Nebulized spray pyrolysis	Pressure-induced continuous tuning of lattice distortion (bond angles) and band gap, pressure induced amorphization and partial recovery upon decompression, forming glass-nanoceramic composite HEO	89
Fluorite (Fm-3m)	$(\text{La},\text{Pr})\text{O}_{2-\delta}$, $(\text{La},\text{Pr},\text{Y})\text{O}_{2-\delta}$, $(\text{Ce},\text{La},\text{Pr})\text{O}_{2-\delta}$, $(\text{Ce},\text{Gd},\text{La},\text{Pr})\text{O}_{2-\delta}$, $(\text{Ce},\text{La},\text{Nd},\text{Pr})\text{O}_{2-\delta}$, $(\text{Ce},\text{La},\text{Pr},\text{Sm})\text{O}_{2-\delta}$, $(\text{Ce},\text{La},\text{Pr},\text{Y})\text{O}_{2-\delta}$,			

TABLE I. (Continued.)

Crystal structure	Compound(s)	Synthesis	Investigated property or application	Reference
Bixbyite (Ia-3), and	(Ce,Gd,La) ₂ O _{3+δ} , (Ce,La,Sm,Y) ₂ O _{3+δ} , (Ce,Gd,La,Pr,Y) ₂ O _{3+δ} , (Ce,La,Pr,Sm,Y) ₂ O _{3+δ} ,	Solid state synthesis	Effect of composition, sintering temperature, sintering atmosphere, and cooling rate on the resulting crystal structure	26
monoclinic (C2/m)	(Gd,La,Sm) ₂ O ₃ , (La,Nd,Y) ₂ O ₃ , (Gd,La,Nd,Sm) ₂ O ₃ , (La,Nd,Sm,Y) ₂ O ₃ , (Gd,La,Sm,Y) ₂ O ₃ , (Gd,La,Nd,Sm,Y) ₂ O ₃ , (Gd,La,Pr,Y) ₂ O ₃ , (La,Pr,Y) ₂ O ₃ , and (La,Gd,Nd,Pr,Sm,Y) ₂ O ₃			
Fluorite (Fm-3m)	Zr _{0.852} Y _{0.148} O _{2-δ} , Hf _{0.284} Zr _{0.284} Ce _{0.284} Y _{0.074} Yb _{0.074} O _{2-δ} , Hf _{0.2} Zr _{0.2} Ce _{0.2} Y _{0.2} Yb _{0.2} O _{2-δ} , Hf _{0.314} Zr _{0.314} Ce _{0.314} Y _{0.029} Ca _{0.029} O _{2-δ} , Hf _{0.284} Zr _{0.284} Ce _{0.284} Y _{0.074} Ca _{0.074} O _{2-δ} , Hf _{0.284} Zr _{0.284} Ce _{0.284} Y _{0.074} Gd _{0.074} O _{2-δ} , Hf _{0.2} Zr _{0.2} Ce _{0.2} Y _{0.2} Gd _{0.2} O _{2-δ} , Hf _{0.314} Zr _{0.314} Ce _{0.314} Y _{0.029} Yb _{0.029} O _{2-δ} , and Hf _{0.314} Zr _{0.314} Ce _{0.314} Y _{0.029} Gd _{0.029} O _{2-δ}	Solid state synthesis	Phase stability, mechanical properties, and thermal conductivities showing increased cubic stability and reduced thermal conductivity while maintaining high modulus and hardness	63
tetragonal				
Spinel (Fd-3m)	(Co _{0.2} Cr _{0.2} Fe _{0.2} Mn _{0.2} Ni _{0.2}) ₃ O ₄	Solid state synthesis	Synthesis method	28
Spinel (Fd-3m)	(Co _{0.2} Cr _{0.2} Fe _{0.2} Mn _{0.2} Ni _{0.2}) ₃ O ₄	Solution combustion synthesis	Lattice parameters, distortion. Magnetization vs magnetic field by powder size	90
Spinel (Fd-3m)	(Cr _{0.2} Fe _{0.2} Mn _{0.2} Ni _{0.2} Zn _{0.2}) ₃ O ₄ (Cr _{0.2} Fe _{0.2} Mn _{0.2} Co _{0.2} Zn _{0.2}) ₃ O ₄ (Cr _{0.2} Fe _{0.2} Mn _{0.2} Co _{0.2} Ni _{0.2}) ₃ O ₄	Glycine-nitrate solution combustion synthesis method	Magnetic properties	59
Spinel (Fd-3m)	(Mg _{0.2} Fe _{0.2} Co _{0.2} Ni _{0.2} Cu _{0.2})Fe ₂ O ₄ , (Mg _{0.2} Co _{0.2} Ni _{0.2} Cu _{0.2} Zn _{0.2})Fe ₂ O ₄ , (Mg _{0.2} Mn _{0.2} Co _{0.2} Ni _{0.2} Cu _{0.2})Fe ₂ O ₄ , (Mn _{0.2} Fe _{0.2} Co _{0.2} Ni _{0.2} Cu _{0.2})Fe ₂ O ₄ , (Cr _{0.2} Mn _{0.2} Fe _{0.2} Co _{0.2} Ni _{0.2}) ₃ O ₄ , (Mg _{0.2} Co _{0.2} Ni _{0.2} Cu _{0.2} Zn _{0.2})Al ₂ O ₄ , (Mg _{0.2} Co _{0.2} Ni _{0.2} Cu _{0.2} Zn _{0.2})Cr ₂ O ₄ , (Mg _{0.2} Fe _{0.2} Co _{0.2} Ni _{0.2} Cu _{0.2})Cr ₂ O ₄ , and (Mg _{0.2} Mn _{0.2} Co _{0.2} Ni _{0.2} Cu _{0.2})Cr ₂ O ₄	Solid state synthesis	Magnetic properties as a function of temperature, charge state	24
Spinel (Fd-3m)	(Co _{0.2} Cr _{0.2} Fe _{0.2} Mn _{0.2} Ni _{0.2}) ₃ O ₄ , (Co _{0.2} Cr _{0.2} Fe _{0.2} Mg _{0.2} Mn _{0.2}) ₃ O ₄ , and (Cr _{0.2} Fe _{0.2} Mg _{0.2} Mn _{0.2} Ni _{0.2}) ₃ O ₄	Solid state synthesis	Seebeck coefficient and electrical conductivity as a function of temperature, phase contents depending on the composition and sintering temperature	91

TABLE I. (Continued.)

Crystal structure	Compound(s)	Synthesis	Investigated property or application	Reference
Spinel (Fd-3m)	$(\text{Co}_{0.2}\text{Cu}_{0.2}\text{Fe}_{0.2}\text{Mn}_{0.2}\text{Ni}_{0.2})_3\text{O}_4$	Solvothermal synthesis followed by annealing	Low-temperature synthesis of small-sized nanoparticles for water oxidation	92
Spinel (Fd-3m)	$(\text{Zn}_{0.2}\text{Fe}_{0.2}\text{Ni}_{0.2}\text{Mg}_{0.2}\text{Cd}_{0.2})\text{Fe}_2\text{O}_4$	Annealing of co-precipitated amorphous precursor	AC electrical conductivity and microwave absorption. Frequency and temperature dependence of dielectric permittivity and magnetic permeability	93
Pyrochlore (Fd-3m)	$(\text{La}_{0.2}\text{Ce}_{0.2}\text{Nd}_{0.2}\text{Sm}_{0.2}\text{Eu}_{0.2})_2\text{Zr}_2\text{O}_7$	Coprecipitation method	Low thermal conductivity and slow grain growth for use as thermal barrier coating	46
Pyrochlore (Fd-3m)	$(\text{La}_{0.2}\text{Nd}_{0.2}\text{Sm}_{0.2}\text{Eu}_{0.2}\text{Gd}_{0.2})_2\text{Zr}_2\text{O}_7$ $(\text{Y}_{0.2}\text{Nd}_{0.2}\text{Sm}_{0.2}\text{Eu}_{0.2}\text{Gd}_{0.2})_2\text{Zr}_2\text{O}_7$ $(\text{La}_{0.2}\text{Y}_{0.2}\text{Sm}_{0.2}\text{Eu}_{0.2}\text{Gd}_{0.2})_2\text{Zr}_2\text{O}_7$ $(\text{La}_{0.2}\text{Nd}_{0.2}\text{Y}_{0.2}\text{Eu}_{0.2}\text{Gd}_{0.2})_2\text{Zr}_2\text{O}_7$ $(\text{La}_{0.2}\text{Nd}_{0.2}\text{Sm}_{0.2}\text{Y}_{0.2}\text{Gd}_{0.2})_2\text{Zr}_2\text{O}_7$ $(\text{La}_{0.2}\text{Nd}_{0.2}\text{Sm}_{0.2}\text{Eu}_{0.2}\text{Y}_{0.2})_2\text{Zr}_2\text{O}_7$	Solid state synthesis	Low thermal conductivity for thermal barrier coating materials	49
Pyrochlore (Fd-3m)	$\text{Gd}_2\text{Zr}_2\text{O}_7$ $(\text{Gd}_{1/2}\text{Eu}_{1/2})_2\text{Zr}_2\text{O}_7$, $(\text{Gd}_{1/3}\text{Eu}_{1/3}\text{Sm}_{1/3})_2\text{Zr}_2\text{O}_7$, $(\text{Gd}_{1/4}\text{Eu}_{1/4}\text{Sm}_{1/4}\text{Nd}_{1/4})_2\text{Zr}_2\text{O}_7$, $(\text{Gd}_{1/5}\text{Eu}_{1/5}\text{Sm}_{1/5}\text{Nd}_{1/5}\text{La}_{1/5})_2\text{Zr}_2\text{O}_7$, $(\text{Gd}_{1/6}\text{Eu}_{1/6}\text{Sm}_{1/6}\text{Nd}_{1/6}\text{La}_{1/6}\text{Dy}_{1/6})_2\text{Zr}_2\text{O}_7$, and $(\text{Gd}_{1/7}\text{Eu}_{1/7}\text{Sm}_{1/7}\text{Nd}_{1/7}\text{La}_{1/7}\text{Dy}_{1/7}\text{Ho}_{1/7})_2\text{Zr}_2\text{O}_7$	Solid state synthesis	Synthesis and verified single phase and homogeneous cation distribution	94
Pyrochlore and defect fluorite	$\text{Sm}_2\text{Zr}_2\text{O}_7$, $\text{Lu}_2\text{Zr}_2\text{O}_7$, $(\text{Sm}_{1/3}\text{Eu}_{1/3}\text{Dy}_{1/3})_2\text{Zr}_2\text{O}_7$, and $(\text{Sm}_{1/5}\text{Eu}_{1/5}\text{Tb}_{1/5}\text{Dy}_{1/5}\text{Lu}_{1/5})_2\text{Zr}_2\text{O}_7$	Co-precipitation followed by solid-state reaction sintering utilizing spark plasma sintering	Thermal expansion, thermal conductivity, mechanical properties, and phase stability for use as thermal barrier coating	62
Mixed pyrochlore and defect fluorite	$(\text{La}_{0.2}\text{Nd}_{0.2}\text{Sm}_{0.2}\text{Gd}_{0.2}\text{Yb}_{0.2})_2\text{Zr}_2\text{O}_7$	Vacuum sintered using combustion nano-powder of transparent	In-line transmittance, Raman and UV-Vis synthesized spectra ceramic	95
Pyrochlore (Fd-3m)	$\text{La}_2(\text{Hf}_{1/2}\text{Zr}_{1/2})_2\text{O}_7$, $\text{Sm}_2(\text{Sn}_{1/4}\text{Ti}_{1/4}\text{Hf}_{1/4}\text{Zr}_{1/4})_2\text{O}_7$ $\text{Gd}_2(\text{Sn}_{1/4}\text{Ti}_{1/4}\text{Hf}_{1/4}\text{Zr}_{1/4})_2\text{O}_7$ $(\text{Sm}_{1/2}\text{Gd}_{1/2})_2(\text{Ti}_{1/3}\text{Hf}_{1/3}\text{Zr}_{1/3})_2\text{O}_7$ $(\text{Eu}_{1/2}\text{Gd}_{1/2})_2(\text{Ti}_{1/3}\text{Hf}_{1/3}\text{Zr}_{1/3})_2\text{O}_7$ $(\text{La}_{1/2}\text{Pr}_{1/2})_2(\text{Sn}_{1/3}\text{Hf}_{1/3}\text{Zr}_{1/3})_2\text{O}_7$ $(\text{Eu}_{1/2}\text{Gd}_{1/2})_2(\text{Sn}_{1/3}\text{Hf}_{1/3}\text{Zr}_{1/3})_2\text{O}_7$ $(\text{La}_{1/3}\text{Pr}_{1/3}\text{Nd}_{1/3})_2(\text{Hf}_{1/2}\text{Zr}_{1/2})_2\text{O}_7$, $(\text{Sm}_{1/3}\text{Eu}_{1/3}\text{Gd}_{1/3})_2(\text{Hf}_{1/2}\text{Zr}_{1/2})_2\text{O}_7$, $(\text{Sm}_{1/3}\text{Eu}_{1/3}\text{Gd}_{1/3})_2(\text{Sn}_{1/3}\text{Hf}_{1/3}\text{Zr}_{1/3})_2\text{O}_7$ $(\text{Sm}_{1/3}\text{Eu}_{1/3}\text{Gd}_{1/3})_2(\text{Ti}_{1/4}\text{Sn}_{1/4}\text{Hf}_{1/4}\text{Zr}_{1/4})_2\text{O}_7$	Solid state synthesis	Thermal conductivity and Young's modulus for use in thermal barrier coating applications. Thermal conductivity correlation with a size disorder parameter investigated as descriptor for thermally insulative material design	61

TABLE I. (Continued.)

Crystal structure	Compound(s)	Synthesis	Investigated property or application	Reference
	$(\text{Sm}_{1/4}\text{Eu}_{1/4}\text{Gd}_{1/4}\text{Yb}_{1/4})_2(\text{Ti}_{1/4}\text{Sn}_{1/4}\text{Hf}_{1/4}\text{Zr}_{1/4})_2\text{O}_7$ $(\text{Sm}_{1/3}\text{Eu}_{1/3}\text{Gd}_{1/3})_2(\text{Ti}_{1/2}\text{Sn}_{1/6}\text{Hf}_{1/6}\text{Zr}_{1/6})_2\text{O}_7$ $(\text{Sm}_{1/3}\text{Eu}_{1/3}\text{Gd}_{1/3})_2(\text{Ti}_{3/4}\text{Sn}_{1/12}\text{Hf}_{1/12}\text{Zr}_{1/12})_2\text{O}_7$, $(\text{Sm}_{1/3}\text{Eu}_{1/3}\text{Gd}_{1/3})_2\text{Ti}_2\text{O}_7$ $(\text{Sm}_{1/4}\text{Eu}_{1/4}\text{Gd}_{1/4}\text{Yb}_{1/4})_2(\text{Ti}_{1/2}\text{Hf}_{1/4}\text{Zr}_{1/4})_2\text{O}_7$ $(\text{Sm}_{3/4}\text{Yb}_{1/4})_2(\text{Ti}_{1/2}\text{Zr}_{1/2})_2\text{O}_7$ $(\text{La}_{1/5}\text{Ce}_{1/5}\text{Nd}_{1/5}\text{Sm}_{1/5}\text{Eu}_{1/5})_2\text{Zr}_2\text{O}_7$ $(\text{La}_{1/7}\text{Ce}_{1/7}\text{Pr}_{1/7}\text{Nd}_{1/7}\text{Sm}_{1/7}\text{Eu}_{1/7}\text{Gd}_{1/7})_2(\text{Hf}_{1/2}\text{Zr}_{1/2})_2\text{O}_7$, $(\text{La}_{1/7}\text{Ce}_{1/7}\text{Pr}_{1/7}\text{Nd}_{1/7}\text{Sm}_{1/7}\text{Eu}_{1/7}\text{Gd}_{1/7})_2(\text{Sn}_{1/3}\text{Hf}_{1/3}\text{Zr}_{1/3})_2\text{O}_7$			
Nanotubes	(TaNbHfZrTi)O	Anodizing HEA precursor	Thermal stability	96
Monoclinic (C12/m1)	$(\text{Yb}_{0.2}\text{Y}_{0.2}\text{Lu}_{0.2}\text{Sc}_{0.2}\text{Gd}_{0.2})_2\text{Si}_2\text{O}_7$	Sol-gel method	Environmental barrier coating (EBC) for SiC-based composites	97
Monoclinic (C2/c)	$(\text{Y}_{1/4}\text{Ho}_{1/4}\text{Er}_{1/4}\text{Yb}_{1/4})_2\text{SiO}_5$	Ball mill and hot press	Use as TEBC material: Young's modulus, thermal conductivity, thermal expansion, and high temperature water vapor resistance	37
Monoclinic (C12/m1)	$(\text{Yb}_{0.25}\text{Y}_{0.25}\text{Lu}_{0.25}\text{Er}_{0.25})_2\text{SiO}_5$	Solid state synthesis	Phase stability and anisotropy in thermal expansion	64
Amorphous glass spheres	(La, Ti, Nb, W, Zr)O	Containerless solidification: Aerodynamic levitation	Hardness and optical properties	98
Magnetoplumbite (P63/mmc)	$(\text{Ba}_{0.7}\text{Sr}_{0.3})(\text{Fe}_{2.9}\text{Al}_{2.5}\text{Mn}_3\text{Ti}_1\text{Ni}_{2.9})\text{O}_{19}$, $(\text{Ba})(\text{Fe}_{5.9}\text{Ti}_{1.3}\text{Cr}_{1.2}\text{Co}_{1.3}\text{Ga}_{1.4}\text{In}_{0.9})\text{O}_{19}$, $(\text{Ba})(\text{Fe}_{5.3}\text{Ti}_{1.5}\text{Al}_{1.4}\text{Cr}_{1.9}\text{Mn}_{1.2}\text{Ni}_{0.7})\text{O}_{19}$, $(\text{Ba})(\text{Fe}_{7.2}\text{Ti}_{0.6}\text{Al}_{0.9}\text{Cr}_{0.7}\text{V}_{0.1}\text{Mn}_{0.3}\text{Co}_{0.3}\text{Ni}_{0.3}\text{Ga}_{0.6})\text{O}_{19}$, $(\text{Ba})(\text{Fe}_{1.4}\text{Ti}_{1.1}\text{Al}_{1.2}\text{Cr}_{1.2}\text{V}_{1.2}\text{Mn}_{1.5}\text{Co}_{1.5}\text{Ni}_{1.3}\text{Ga}_{1.1})\text{O}_{19}$, $(\text{Ba}_{0.5}\text{Sr}_{0.2}\text{La}_{0.2}\text{Ca}_{0.1})(\text{Fe}_{12})\text{O}_{19}$, and $(\text{Ba}_{0.44}\text{Sr}_{0.33}\text{La}_{0.23})(\text{Fe}_{2.7}\text{Al}_{2.7}\text{Cr}_{2.7}\text{Ga}_{2.3}\text{In}_{1.3})\text{O}_{19}$	Solid state synthesis	Microstructure and magnetization	99
Magnetoplumbite (P63/mmc)	$(\text{Ba}_1)(\text{Fe}_{5.83}\text{Al}_{1.19}\text{Ti}_{1.08}\text{Cr}_{1.12}\text{Cu}_{0.78}\text{Ga}_{1.03}\text{In}_{0.97})\text{O}_{19}$	Solid state synthesis	Structure and magnetic properties with temperature	100
Rutile (P42/mnm)	$(\text{Al}_{0.19}\text{Cr}_{0.13}\text{Nb}_{0.19}\text{Ta}_{0.30}\text{Ti}_{0.19})\text{O}_2$	Reactive magnetron sputtering	Hardness and indentation moduli as a function of relative oxygen flow rate	101
Non-crystalline films	FeCoNiO _x , CrFeCoNiO _x , AlFeCoNiO _x , and TiFeCoNiO _x	Arc melting and physical vapor deposition	Microstructures and electrical resistivity	102

TABLE I. (Continued.)

Crystal structure	Compound(s)	Synthesis	Investigated property or application	Reference
Mixed phase spinel, BCC, and FCC nanoparticles	Five elements (Ni, Fe, Co, Cr, and Al) and oxygen	Sol–gel auto-combustion method and then used as the catalyst for the growth of CNTs by the chemical vapor deposition technique	Utilization of HEO nanoparticles as a cost-effective catalyst for the growth of high yield carbon nanotubes for energy applications, such as electrochemical capacitors	103
...	A case study with $\text{LaMnO}_{3\pm\delta}$	Defect chemistry analysis and calculation of phase diagram (CALPHAD) approach	Exploration of high entropy ceramics with computational thermodynamics	104

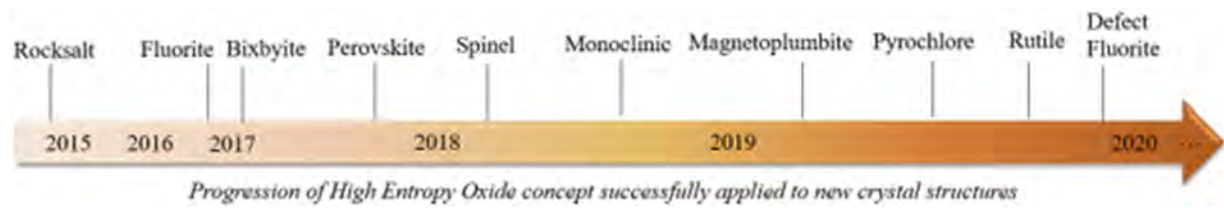


FIG. 2. Timeline representing the expansion of high entropy oxides to other crystal systems since their realization with the rock salt structure in 2015.

In summary

- Evidence supports that high configurational entropy of mixing is a contributing factor to the formation of a single-phase solid solution, but not exclusively.
- Work on rare-earth HEOs shows evidence that particular element additions can be a stabilizing factor.²⁹
- Minimization of Gibbs free energy to achieve single-phase stability benefits from configurational entropy maximization via the mixing of many diverse element species.
- For the case of oxides, it has been stated that there should be appropriately diverse structures, coordination, and cationic radii to directly test whether entropy is a dominant factor in stabilizing solid solutions.

III. STUDIES AND OUTLOOK FOR IMPROVED PROPERTIES AND FUNCTIONALITY

A. Local structure and computational and prediction models

A defining characteristic of the ideal HEO in the current literature is the attainment of a single, pure phase. Almost all HEO structure characterization efforts to date have included laboratory x-ray diffraction (XRD) or Selected Area Electron Diffraction (SAED) to identify the crystal structure type, determine the phase purity, and assess the overall crystallinity. Only a few studies to date have included quantitative (full profile) refinements of diffraction data

in detail^{20,30} with fewer still utilizing data from high resolution³¹ or neutron^{32,33} instruments.

Random and homogeneous cation distribution on a single sublattice site with no evidence of chemical clustering or local distortion is commonly discussed in the literature as a second defining characteristic of an ideal HEO. Advanced microscopy probes, including high angle annular dark-field (HAADF) and annular bright-field (ABF) imaging, aberration-corrected scanning transmission electron microscopy (STEM), energy dispersive x-ray spectroscopy (EDX), and electron energy loss spectroscopy (EELS), have been applied in numerous cases to examine to what extent multiple cations are homogeneously and randomly dispersed.^{8,20,25,31,34–38} Atom probe tomography (APT) has recently been successfully applied³⁰ to this area as well. There have been a few studies involving local structure probes to further explore cation arrangement and local atomic (and in some cases spin) disorder in HEOs, including extended x-ray absorption fine structure (EXAFS),^{8,38,39} x-ray and neutron pair distribution function (PDF),³³ Raman spectroscopy,³⁴ electron paramagnetic resonance (EPR),⁴⁰ nuclear magnetic resonance (NMR),³⁶ Mössbauer spectroscopy,⁴¹ and neutron spectroscopy.³³ There is still much to be discovered: What is the nature and extent of chemical short-range order among HEO cations? To what extent do random vs ordered cation arrays impact the entropy/stability and properties of systems? What are the local environments (defects and distortions) surrounding specific ions? In addition, to what extent do these features impact the entropy/stability of HEO systems?

Closely integrated experiment and theory will be indispensable for gaining comprehensive insights into HEO structural archetypes and their properties. The prototypical rock salt type HEO (MgCoNiCuZn)O is by far the most comprehensively characterized to date, presenting an early case study. In their initial report, Rost *et al.* concluded through application of a variety of techniques that the cations are uniformly and randomly dispersed.⁸ Detailed EXAFS and Density Functional Theory (DFT) work revealed Cu²⁺ local Jahn–Teller type distortions (four short and two long copper–oxygen bond lengths) accommodated via uncorrelated oxygen sublattice disorder.^{42,43} This group and others (for example, Ref. 40) have demonstrated that the distortions can be reduced or removed by eliminating Cu from rock salt compositions.

Even with the application of multiple data types, rigorous statistical and computational techniques, and complex atomistic modeling, the determination of true local atomic structure in HEOs and related materials will stretch the abilities of modern techniques and practitioners. Researchers should remain cautious in interpreting properties and trends in HEOs based on reported or determined atomistic structures, bearing in mind the sensitivities and limits of the specific structural probes and modeling approaches applied, and also the certainty that various synthesis approaches, processing conditions, and material uses will impart variations in local atomic structure features for any fixed HEO composition.

B. Optical materials

The band gap results reported in the rare-earth HEO work show that having a combination of Ce and multivalent Pr helps to achieve a single phase while reducing the band gap (~ 2 eV), enabling light absorption over the entire visible range.²⁹ This creates a more flexible method for engineering the oxygen vacancy concentration as well as offering element-based property tuning without sacrificing phase purity or visible light absorbing capability. Further experimental studies should be done in parallel with theoretical modeling of the electronic structure to elucidate the band structure of HEOs. Studies of surface diffusion effects and compositional gradient effects on optical properties with this new class of materials could also be an avenue to pursue. The band gap tunability could lead to interesting applications in optical materials as well as the development of new scintillators and lasers.

C. Electronic properties

1. Ionic conductivity

The observed colossal dielectric constants and the superior ionic conductivities achieved in Bérardan's work with (Mg, Co, Ni, Cu, Zn)_{1-x}Li_xO, (Mg, Co, Ni, Cu, Zn)_{1-x}Na_xO, (Mg, Co, Ni, Cu, Zn)_{1-2x}Li_xGa_xO, and (Mg, Co, Ni, Cu, Zn)_{0.95}K_{0.05}O samples show that larger ionic conductivity values can be obtained by optimizing the concentration and/or ordering of oxygen vacancies along with the size of the divalent cations in the compound. This demonstrates the potential of HEOs as novel materials for solid-state battery applications.²⁷ Recent work has shown that disorder within a crystal lattice can play a dominant role in improving the ion conductivity in solid electrolytes⁴⁴ and suggests that HEOs may provide exceptionally high ion conductivities.

2. Thermal conductivity and thermoelectrics

The lower limit to the intrinsic thermal conductivity of a solid is assumed to be the amorphous thermal conductivity.⁴⁵ Low thermal conductivity is of interest for thermoelectric power generation and thermal barrier coatings, and nearing the amorphous limit is a desirable trait for applications in these areas. Several HEOs studied thus far indicate that a low thermal conductivity approaching the amorphous limit may be typical for these compounds.^{21,34,46–50} As the entropy stabilization of the multiple cations reduces the phonon scattering time rather than velocity, it allows for the possibility of high modulus materials with low thermal conductivity, offering the opportunity for new property combinations. A study on the effects of a sixth cation species addition to a rock salt HEO and its subsequent reduction in thermal conductivity was reported by Braun *et al.*⁴⁷ The thermal conductivity is usually reduced at the expense of an increase in stiffness (elastic modulus), however, Braun's EXAFS work shows that the reduction in thermal conductivity in the rock salt HEOs is due to atomic level disorder resulting from a charge difference among the cations, with the local disorder distorting the oxygen sublattice and preserving a long range order as seen in XRD.⁴⁷ A study conducted on single-crystal films of Ba(Zr_{0.2}Sn_{0.2}Ti_{0.2}Hf_{0.2}Nb_{0.2})O₃ shows very low thermal conductivity, with the thermal conductivity of the film grown on MgO reported to be 0.58 ± 0.03 W/mK and that on SrTiO₃ reported to be 0.54 ± 0.04 W/mK.³⁴ These values are very close to the theoretical amorphous limit of cubic phase BaTiO₃, which is estimated at ~ 0.48 W/mK.^{45,51} This is especially noteworthy, since the material still possesses a configurationally ordered A-site sublattice, and supports the theoretical prediction that highly configurationally disordered single crystals might provide an avenue to approach the amorphous limit.³⁴

Since the thermoelectric figure of merit, ZT, scales with the operational temperature, the high thermal stability of high entropy materials means that they may be able to operate at high temperatures, increasing their figure of merit. While there have been some investigations of the thermoelectric properties of high entropy alloys (metals), there have been comparably few in high entropy oxides. However, it was reported that oxides are particularly promising for thermoelectric applications,⁵² indicating that there are significant opportunities in the field. There are practical advantages specifically for high entropy materials, as many of the high entropy materials are made from common elements, making them affordable and scalable. This is a particularly crucial point since cost has been identified as a particular barrier to the practical development of thermoelectric devices. Also, many of the practical applications of thermoelectrics are predicated on taking thermal energy radiated to the environment as waste and recovering it as electrical currents. These applications frequently necessitate operation at high temperatures, again promoting high entropy materials as promising candidates for practical thermoelectrics due to their high thermal stability.⁵³ These factors taken together suggest that there are significant opportunities to discover highly efficient thermoelectric materials in high entropy oxides, which can easily be transferred to practical devices and applications.

3. Ferroelectrics

The ability to minutely control how a material responds to an applied electric or electromagnetic field is critical to applications.

While there is little published work directly related to applying HEOs to the discovery of new ferroelectric, relaxor, or dielectric properties, there are several reasons to believe that this is one area where we should expect fast growth. The ability to stabilize a range of desired crystal structures with highly tunable cation composition opens many new opportunities from an engineering standpoint. There are also some interesting fundamental questions, which might be uniquely addressed with these new materials. As an example, disorder in ferroelectric materials is well studied as it relates to the formation of morphotropic phases and impact on domain wall formation and propagation. In these instances, disorder is generally treated as near point-like or as a local cluster in a broadly uniform matrix, which can be used to seed macroscopic phases and dictate phase dynamics. What happens when the disorder is uniformly distributed throughout the lattice? Low hanging fruit in this area is likely in the realm of relaxor ferroelectrics,³⁴ where changing disorder within the lattice can have a dominating role in crystal phase metastabilities and Curie temperatures.⁵⁴

4. Strongly correlated electrons

A virtually untapped area where HEO materials can be expected to have a significant impact is in the field of strongly correlated materials. These materials possess exceptionally valuable functional properties, such as high temperature superconductivity, metal-to-insulator transitions, and colossal magnetic response; however, they are generally poorly understood from a fundamental standpoint. In these systems, the nearly degenerate energy scales of materials' spin, orbital, and charge order parameters lead to extraordinary sensitivity to even minute changes of chemical composition or lattice deformation. Local chemical disorder is known to play an important or even dominating role in the emergence of functionality, yet there are surprisingly few studies aimed at gaining specific knowledge of disorder's role. This is partly the result of difficulty stabilizing quaternary or higher order crystals, which may now be overcome through entropy stabilization approaches and lead to unexpected behaviors. As an example, recent work in HEO systems has demonstrated that even in exceptionally disordered crystalline materials long range magnetic order can emerge.^{31,38,41,56} How does the extreme local disorder lead to macroscopic order, and what other long-range collective behaviors might also emerge? There is also a great deal of promise in considering how these materials might be used in quantum materials applications. As examples, the ability to finely tune disorder may enable easy access to quantum critical points,⁵⁶ while controlling cation compositions for specific magnetic exchange interaction pathways could open new levels of control over spin textured states.⁵⁷ Stabilization of single crystals comprised of 5 or more cations in increasingly complex and reduced symmetry crystal structures opens an extraordinary new phase space in which we can expect to find many unexpected exotic behaviors.

D. Magnetic properties

Despite the increasing number of HEO materials being synthesized and studied, magnetic properties have only recently started to attract attention. Inducing disorder often gives rise to lattice distortion, octahedral tilting, and changes in electronegativity that can

all influence exchange interactions and magnetic behavior, making high entropy materials fertile ground for tuning and discovering interesting or exotic magnetic properties.

Recent studies on the nature of magnetism in $(\text{Mg}_{0.2}\text{Co}_{0.2}\text{Ni}_{0.2}\text{Cu}_{0.2}\text{Zn}_{0.2})\text{O}$ hint at a more complicated structure–property picture. This material features a broad transition to long-range antiferromagnetic order below ~ 113 K, in a manner consistent with a randomized and homogeneous cation distribution of the three constituent magnetic ions.^{32,33} However, certain characteristics of the transition (magnetic susceptibility deviating from the Curie–Weiss behavior, absence of anomalies in heat capacity, and strong magnetic excitations surviving up to room temperature) are consistent with local magnetic fluctuations typically associated with chemical clustering.³³ Regardless, Meisenheimer and co-workers, in recent work including DFT, EXAFS, and magnetization studies, demonstrated that the Cu^{2+} concentration and associated “stereochemically driven structural disorder” can be used to tune lattice, charge, and spin disorder in thin film samples, all while retaining high phase purity and crystallinity.³⁸ The study of the exchange bias phenomena seen in a rock salt HEO with varying concentration of Co, $(\text{Mg}_{0.25(1-x)}\text{Co}_x\text{Cu}_{0.25(1-x)}\text{Ni}_{0.25(1-x)}\text{Zn}_{0.25(1-x)})\text{O}$ ($x = 0.2, 0.27, \text{ and } 0.33$), shows that the unique properties of HEO materials can be utilized to tailor the magnetic phenomena in oxide thin films.⁵⁸

Recent DC and AC magnetometry and Mössbauer spectra reported for rare-earth and transition metal HEO perovskites, $(\text{Gd, La, Nd, Sm, and/or Y})(\text{Co, Cr, Fe, Mn, and/or Ni})\text{O}_3$, show a relationship between the magnetic exchange and the chemical disorder, with a predominant antiferromagnetic behavior with small ferromagnetic contribution.⁴¹ In studies on the spinel system, the iron-based compounds have shown room temperature ferromagnetic ordering with tunable saturation, coercivity, and transition temperature.^{24,59} X-ray absorption spectroscopy and x-ray magnetic linear dichroism for $(\text{Mg}_{0.2}\text{Mn}_{0.2}\text{Co}_{0.2}\text{Ni}_{0.2}\text{Cu}_{0.2})\text{Fe}_2\text{O}_4$, $(\text{Mn}_{0.2}\text{Fe}_{0.2}\text{Co}_{0.2}\text{Ni}_{0.2}\text{Cu}_{0.2})\text{Fe}_2\text{O}_4$, and $(\text{Mg}_{0.2}\text{Fe}_{0.2}\text{Co}_{0.2}\text{Ni}_{0.2}\text{Cu}_{0.2})\text{Cr}_2\text{O}_4$ show evidence of antiferromagnetic ordering and identified the unexpected presence of Cr^{4+} in $(\text{Mg}_{0.2}\text{Fe}_{0.2}\text{Co}_{0.2}\text{Ni}_{0.2}\text{Cu}_{0.2})\text{Cr}_2\text{O}_4$.²⁴ Low temperature magnetometry on $(\text{Mg}_{0.2}\text{Fe}_{0.2}\text{Co}_{0.2}\text{Ni}_{0.2}\text{Cu}_{0.2})\text{Cr}_2\text{O}_4$ showed large coercivity, while $(\text{Mg}_{0.2}\text{Mn}_{0.2}\text{Co}_{0.2}\text{Ni}_{0.2}\text{Cu}_{0.2})\text{Fe}_2\text{O}_4$ exhibited a slight exchange bias and a lack of saturation even in 9 T fields. Work on single crystal films of $\text{La}(\text{Cr}_{0.2}\text{Mn}_{0.2}\text{Fe}_{0.2}\text{Co}_{0.2}\text{Ni}_{0.2})\text{O}_3$ suggests the presence of long-range magnetic order in a disordered material and reveals that magnetic properties are strongly dependent on substrate-induced lattice anisotropy.⁵⁵ The possibility of manipulating magnetic properties through lattice symmetry adds a new approach to the design of desired magnetic responses.⁵⁵

Due to the presence of multiple metallic elements in many HEO materials, a range of magnetic applications can be envisioned, including rare-earth-free permanent magnets. New spin liquids, characterized by long-range quantum entanglement and the absence of magnetic ordering, and spin glasses, with magnetic moments “frozen” in a disordered pattern, are possibilities in entropy-stabilized oxides. In the case of the spinel structure, cation selection will determine possible site inversion, adding another degree of complexity. Further study on other compositions and structures of magnetic HEO materials should be conducted both in bulk and film materials.

E. Mechanical properties

Studies of HEAs have mainly focused on their applications as structural materials. With the advent of HEOs, the possibility of non-metallic structural materials should also be pursued, as the disorder inherent to HEOs could lead to improved mechanical properties, as is the case in HEAs.⁷ Mechanical properties of the newly developed bulk HEOs have been investigated in the rock salt system to discover a trade-off between densification and grain growth, reporting a maximum bending strength of 323 MPa and elastic modulus of 108 GPa.⁶⁰ Mechanical properties of silicate HEOs and high and medium entropy pyrochlores have started to be investigated for applications in thermal barrier coatings.^{37,49,61–63} HEOs could offer applications in wear resistant coatings, in materials for cutting tools, and high temperature structural components, warranting further investigation of the mechanical properties. A new class of high-entropy transparent ceramics (rare-earth-alkaline-earth metal fluoride) in the form of CeNdCaSrBaF₁₂ shows significant potential for a range of new functionalities, including use as a laser ceramic with unique chemistry and optical properties that are considerably different from those found in conventional fluoride transparent ceramics.¹² The successful synthesis of a disordered transparent ceramic shows opportunity for the development of transparent HEOs and could provide an avenue for developing enhanced infrared windows and bulletproof glasses.

F. Thermal expansion

While the thermal expansion behavior has only started to be investigated in a few high entropy silicates and pyrochlores,^{37,46,64} the high degree of tunability offered by HEOs is expected to provide an avenue for modifying thermal expansion through cation selection. HEOs also offer the opportunity to discover new materials with anomalously low or negative thermal expansion. The Invar effect caused by thermal excitations between two possible magnetic states is believed to compensate for the lattice expansion related to anharmonic effects of the lattice vibrations.⁶⁵ In studies of one such Invar alloy system, Fe–Ni, it has been suggested that the disordered local moment model accounts for the possibility of antiparallel spin alignments and the presence of multiple magnetic states.⁶⁵ In the case of HEO systems, the high level of disorder and the presence of multiple magnetic constituents could lead to unique thermal expansion behavior with competition between the magnetic and crystal lattice.

IV. CONCLUDING REMARKS

By utilizing entropy as the driving force for engineering oxide materials, the deviation from traditional prediction methods and principles offers a path for new structure–property relations to be discovered and innovative HEO structures and subsequent properties to be explored. The multi-cation approach inherent to high entropy oxides allows for the tailoring of physical properties to meet the requirements of the application. While HEOs offer significant opportunities for functional material applications, their intrinsic disorder and highly localized chemical environments bring along new challenges. Deeper investigation should be performed, with the support of theoretical work and a variety of local to long-range probes,

to gain understanding of the effects the disorder has on the structure and ordering to uncover and ultimately utilize the tremendous possibilities of functional HEOs.

ACKNOWLEDGMENTS

T.Z.W., D.G., D.M., E.P., E.G., and J.Y. acknowledge the support from the U.S. Department of Energy (DOE), Office of Science, Basic Energy Sciences, Materials Sciences and Engineering Division. B.L.M. acknowledges the support from the Center for Materials Processing, a Tennessee Higher Education Commission (THEC) supported Accomplished Center of Excellence.

REFERENCES

- J.-W. Yeh, S.-K. Chen, S.-J. Lin, J.-Y. Gan, T.-S. Chin, T.-T. Shun, C.-H. Tsau, and S.-Y. Chang, *Adv. Eng. Mater.* **6**, 299 (2004).
- B. Cantor, I. T. H. Chang, P. Knight, and A. J. B. Vincent, *Mater. Sci. Eng. A* **375–377**, 213 (2004).
- E. P. George, D. Raabe, and R. O. Ritchie, *Nat. Rev. Mater.* **4**, 515 (2019).
- M. C. Gao, D. B. Miracle, D. Maurice, X. Yan, Y. Zhang, and J. A. Hawk, *J. Mater. Res.* **33**, 3138 (2018).
- L. Sun and R. J. Cava, *Phys. Rev. Mater.* **3**, 090301 (2019).
- N. Dragoie and D. Bérardan, *Science* **366**, 573 (2019).
- D. B. Miracle and O. N. Senkov, *Acta Mater.* **122**, 448 (2017).
- C. M. Rost, E. Sachet, T. Borman, A. Moballegh, E. C. Dickey, D. Hou, J. L. Jones, S. Curtarolo, and J.-P. Maria, *Nat. Commun.* **6**, 8485 (2015).
- J. Gild, Y. Zhang, T. Harrington, S. Jiang, T. Hu, M. C. Quinn, W. M. Mellor, N. Zhou, K. Vecchio, and J. Luo, *Sci. Rep.* **6**, 37946 (2016).
- J. Zhou, J. Zhang, F. Zhang, B. Niu, L. Lei, and W. Wang, *Ceram. Int.* **44**, 22014 (2018).
- R.-Z. Zhang, F. Gucci, H. Zhu, K. Chen, and M. J. Reece, *Inorg. Chem.* **57**, 13027 (2018).
- X. Chen and Y. Wu, *J. Am. Ceram. Soc.* **103**, 750 (2020).
- T. Wen, H. Liu, B. Ye, D. Liu, and Y. Chu, *Sci. China Mater.* **63**, 300 (2020).
- M. Lorenz, M. S. Ramachandra Rao, T. Venkatesan, E. Fortunato, P. Barquinha, R. Branquinho, D. Salgueiro, R. Martins, E. Carlos, A. Liu, F. K. Shan, M. Grundmann, H. Boscher, J. Mukherjee, M. Priyadarshini, N. DasGupta, D. J. Rogers, F. H. Teherani, E. V. Sandana, P. Bove, K. Rietwyk, A. Zaban, A. Veziridis, A. Weidenkaff, M. Muralidhar, M. Murakami, S. Abel, J. Fompeyrine, J. Zuniga-Perez, R. Ramesh, N. A. Spaldin, S. Ostanin, V. Borisov, I. Mertig, V. Lazenka, G. Srinivasan, W. Prellier, M. Uchida, M. Kawasaki, R. Pentcheva, P. Gegenwart, F. Miletto Granozio, J. Fontcuberta, and N. Pryds, *J. Phys. D: Appl. Phys.* **49**, 433001 (2016).
- A. Sarkar, Q. Wang, A. Schiele, M. R. Chellali, S. S. Bhattacharya, D. Wang, T. Brezesinski, H. Hahn, L. Velasco, and B. Breitung, *Adv. Mater.* **31**, 1806236 (2019).
- F. Otto, Y. Yang, H. Bei, and E. P. George, *Acta Mater.* **61**, 2628 (2013).
- F. Otto, A. Dlouhý, K. G. Pradeep, M. Kuběnová, D. Raabe, G. Eggeler, and E. P. George, *Acta Mater.* **112**, 40 (2016).
- B. Schuh, F. Mendez-Martin, B. Völker, E. P. George, H. Clemens, R. Pippan, and A. Hohenwarter, *Acta Mater.* **96**, 258 (2015).
- A. D. Dupuy, X. Wang, and J. M. Schoenung, *Mater. Res. Lett.* **7**, 60 (2019).
- A. Sarkar, R. Djenadic, D. Wang, C. Hein, R. Kautenburger, O. Clemens, and H. Hahn, *J. Eur. Ceram. Soc.* **38**, 2318 (2018).
- K. Chen, X. Pei, L. Tang, H. Cheng, Z. Li, C. Li, X. Zhang, and L. An, *J. Eur. Ceram. Soc.* **38**, 4161 (2018).
- R. Djenadic, A. Sarkar, O. Clemens, C. Loh, M. Botros, V. S. K. Chakravadhanula, C. Kübel, S. S. Bhattacharya, A. S. Gandhi, and H. Hahn, *Mater. Res. Lett.* **5**, 102 (2017).
- Z. Wu, H. Bei, F. Otto, G. M. Pharr, and E. P. George, *Intermetallics* **46**, 131 (2014).

- ²⁴B. Musicó, Q. Wright, T. Z. Ward, A. Grutter, E. Arenholz, D. Gilbert, D. Mandrus, and V. Keppens, *Phys. Rev. Mater.* **3**, 104416 (2019).
- ²⁵S. Jiang, T. Hu, J. Gild, N. Zhou, J. Nie, M. Qin, T. Harrington, K. Vecchio, and J. Luo, *Scr. Mater.* **142**, 116 (2018).
- ²⁶M. Pianassola, M. Loveday, J. W. McMurray, M. Koschan, C. L. Melcher, and M. Zhuravleva, *J. Am. Ceram. Soc.* **10**, 16971 (2020).
- ²⁷D. Bérardan, S. Franger, D. Dragoe, A. K. Meena, and N. Dragoe, *Phys. Status Solidi - Rapid Res. Lett.* **10**, 328 (2016).
- ²⁸J. Dąbrowa, M. Stygar, A. Mikula, A. Knapik, K. Mroczka, W. Tejchman, M. Danielewski, and M. Martin, *Mater. Lett.* **216**, 32 (2018).
- ²⁹A. Sarkar, C. Loho, L. Velasco, T. Thomas, S. S. Bhattacharya, H. Hahn, and R. Djenadic, *Dalt. Trans.* **46**, 12167 (2017).
- ³⁰M. R. Chellali, A. Sarkar, S. H. Nandam, S. S. Bhattacharya, B. Breitung, H. Hahn, and L. Velasco, *Scr. Mater.* **166**, 58 (2019).
- ³¹K. P. Tseng, Q. Yang, S. J. McCormack, and W. M. Kriven, *J. Am. Ceram. Soc.* **103**, 569 (2020).
- ³²M. P. Jimenez-Segura, T. Takayama, D. Bérardan, A. Hoser, M. Reehuis, H. Takagi, and N. Dragoe, *Appl. Phys. Lett.* **114**, 122401 (2019).
- ³³J. Zhang, J. Yan, S. Calder, Q. Zheng, M. A. McGuire, D. L. Abernathy, Y. Ren, S. H. Lapidus, K. Page, H. Zheng, J. W. Freeland, J. D. Budai, and R. P. Hermann, *Chem. Mater.* **31**, 3705 (2019).
- ³⁴Y. Sharma, B. L. Musico, X. Gao, C. Hua, A. F. May, A. Herklotz, A. Rastogi, D. Mandrus, J. Yan, H. N. Lee, M. F. Chisholm, V. Keppens, and T. Z. Ward, *Phys. Rev. Mater.* **2**, 060404 (2018).
- ³⁵F. Okejiri, Z. Zhang, J. Liu, M. Liu, S. Yang, and S. Dai, *ChemSusChem* **13**, 111 (2020).
- ³⁶Q. Wang, A. Sarkar, D. Wang, L. Velasco, R. Azmi, S. S. Bhattacharya, T. Bergfeldt, A. Düvel, P. Heitjans, T. Brezesinski, H. Hahn, and B. Breitung, *Energy Environ. Sci.* **12**, 2433 (2019).
- ³⁷X. Ren, Z. Tian, J. Zhang, and J. Wang, *Scr. Mater.* **168**, 47 (2019).
- ³⁸P. B. Meisenheimer, L. D. Williams, S. H. Sung, J. Gim, P. Shafer, G. N. Kotsonis, J. Maria, M. Trassin, R. Hovden, E. Kioupakis, and J. T. Heron, *Phys. Rev. Mater.* **3**, 104420 (2019).
- ³⁹H. Chen, W. Lin, Z. Zhang, K. Jie, D. R. Mullins, X. Sang, S.-Z. Yang, C. J. Jafta, C. A. Bridges, X. Hu, R. R. Unocic, J. Fu, P. Zhang, and S. Dai, *ACS Mater. Lett.* **1**, 83 (2019).
- ⁴⁰D. Bérardan, A. K. Meena, S. Franger, C. Herrero, and N. Dragoe, *J. Alloys Compd.* **704**, 693 (2017).
- ⁴¹R. Witte, A. Sarkar, R. Kruk, B. Eggert, R. A. Brand, H. Wende, and H. Hahn, *Phys. Rev. Mater.* **3**, 034406 (2019).
- ⁴²C. M. Rost, Z. Rak, D. W. Brenner, and J.-P. Maria, *J. Am. Ceram. Soc.* **100**, 2732 (2017).
- ⁴³Z. Rák, J.-P. Maria, and D. W. Brenner, *Mater. Lett.* **217**, 300 (2018).
- ⁴⁴G. K. Phani Dathar, J. Balachandran, P. R. C. Kent, A. J. Rondinone, and P. Ganesh, *J. Mater. Chem. A* **5**, 1153 (2017).
- ⁴⁵D. G. Cahill, S. K. Watson, and R. O. Pohl, *Phys. Rev. B* **46**, 6131 (1992).
- ⁴⁶Z. Zhao, H. Xiang, F.-Z. Dai, Z. Peng, and Y. Zhou, *J. Mater. Sci. Technol.* **35**, 2647 (2019).
- ⁴⁷J. L. Braun, C. M. Rost, M. Lim, A. Giri, D. H. Olson, G. N. Kotsonis, G. Stan, D. W. Brenner, J.-P. Maria, and P. E. Hopkins, *Adv. Mater.* **30**, 1805004 (2018).
- ⁴⁸A. Giri, J. L. Braun, C. M. Rost, and P. E. Hopkins, *Scr. Mater.* **138**, 134 (2017).
- ⁴⁹F. Li, L. Zhou, J.-X. Liu, Y. Liang, and G.-J. Zhang, *J. Adv. Ceram.* **8**, 576 (2019).
- ⁵⁰M. Lim, Z. Rak, J. L. Braun, C. M. Rost, G. N. Kotsonis, P. E. Hopkins, J.-P. Maria, and D. W. Brenner, *J. Appl. Phys.* **125**, 055105 (2019).
- ⁵¹S. Kashida, I. Hatta, A. Ikushima, and Y. Yamada, *J. Phys. Soc. Jpn.* **34**, 997 (1973).
- ⁵²K. Koumoto, I. Terasaki, and R. Funahashi, *Mater. Res. Bull.* **31**, 206 (2006).
- ⁵³S. Funahashi, S. Guo, Q. Hu, H. Fahlquist, P. Erhart, and A. Palmqvist, *J. Appl. Phys.* **118**, 184905 (2015).
- ⁵⁴N. Setter and L. E. Cross, *J. Appl. Phys.* **51**, 4356 (1980).
- ⁵⁵Y. Sharma, Q. Zheng, A. R. Mazza, E. Skoropata, T. Heitmann, Z. Gai, B. Musico, P. F. Miceli, B. C. Sales, V. Keppens, M. Brahele, and T. Z. Ward, *Phys. Rev. Mater.* **4**, 014404 (2020).
- ⁵⁶T. Goko, C. J. Arguello, A. Hamann, T. Wolf, M. Lee, D. Reznik, A. Maisuradze, R. Khasanov, E. Morenzoni, and Y. J. Uemura, *npj Quantum Mater.* **2**, 44 (2017).
- ⁵⁷A. Scaramucci, H. Shinaoka, M. V. Mostovoy, M. Müller, C. Mudry, M. Troyer, and N. A. Spaldin, *Phys. Rev. X* **8**, 011005 (2018).
- ⁵⁸P. B. Meisenheimer, T. J. Kratoch, and J. T. Heron, *Sci. Rep.* **7**, 13344 (2017).
- ⁵⁹A. Mao, H.-Z. Xiang, Z.-G. Zhang, K. Kuramoto, H. Zhang, and Y. Jia, *J. Magn. Magn. Mater.* **497**, 165884 (2020).
- ⁶⁰W. Hong, F. Chen, Q. Shen, Y. Han, W. G. Fahrenholtz, and L. Zhang, *J. Am. Ceram. Soc.* **375**, 213 (2018).
- ⁶¹A. J. Wright, Q. Wang, S.-T. Ko, K. M. Chung, R. Chen, and J. Luo, *Scr. Mater.* **181**, 76 (2020).
- ⁶²K. Ren, Q. Wang, G. Shao, X. Zhao, and Y. Wang, *Scr. Mater.* **178**, 382 (2020).
- ⁶³A. J. Wright, Q. Wang, C. Huang, A. Nieto, R. Chen, and J. Luo, *J. Eur. Ceram. Soc.* **40**, 2120 (2019).
- ⁶⁴H. Chen, H. Xiang, F.-Z. Dai, J. Liu, and Y. Zhou, *J. Mater. Sci. Technol.* **36**, 134 (2020).
- ⁶⁵M. van Schilfhaar, I. A. Abrikosov, and B. Johansson, *Nature* **400**, 46 (1999).
- ⁶⁶A. Sarkar, R. Djenadic, N. J. Usharani, K. P. Sanghvi, V. S. K. Chakravadhanula, A. S. Gandhi, H. Hahn, and S. S. Bhattacharya, *J. Eur. Ceram. Soc.* **37**, 747 (2017).
- ⁶⁷D. Bérardan, S. Franger, A. K. Meena, and N. Dragoe, *J. Mater. Chem. A* **4**, 9536 (2016).
- ⁶⁸A. Sarkar, L. Velasco, D. Wang, Q. Wang, G. Talasila, L. de Biasi, C. Kübel, T. Brezesinski, S. S. Bhattacharya, H. Hahn, and B. Breitung, *Nat. Commun.* **9**, 3400 (2018).
- ⁶⁹H. Chen, J. Fu, P. Zhang, H. Peng, C. W. Abney, K. Jie, X. Liu, M. Chi, and S. Dai, *J. Mater. Chem. A* **6**, 11129 (2018).
- ⁷⁰M. Biesuz, L. Spiridigliozzi, G. Dell'Agli, M. Bortolotti, and V. M. Sglavo, *J. Mater. Sci.* **53**, 8074 (2018).
- ⁷¹Z. Rak, C. M. Rost, M. Lim, P. Sarker, C. Toher, S. Curtarolo, J.-P. Maria, and D. W. Brenner, *J. Appl. Phys.* **120**, 095105 (2016).
- ⁷²G. N. Kotsonis, C. M. Rost, D. T. Harris, and J.-P. Maria, *MRS Commun.* **8**, 1371 (2018).
- ⁷³Q. Wang, A. Sarkar, Z. Li, Y. Lu, L. Velasco, S. S. Bhattacharya, T. Brezesinski, H. Hahn, and B. Breitung, *Electrochem. Commun.* **100**, 121 (2019).
- ⁷⁴N. Qiu, H. Chen, Z. Yang, S. Sun, Y. Wang, and Y. Cui, *J. Alloys Compd.* **777**, 767 (2019).
- ⁷⁵Z.-M. Yang, K. Zhang, N. Qiu, H.-B. Zhang, Y. Wang, and J. Chen, *Chin. Phys. B* **28**, 046201 (2019).
- ⁷⁶N. Osenciat, D. Bérardan, D. Dragoe, B. Léridon, S. Holé, A. K. Meena, S. Franger, and N. Dragoe, *J. Am. Ceram. Soc.* **102**, 6156 (2019).
- ⁷⁷J. Chen, W. Liu, J. Liu, X. Zhang, M. Yuan, Y. Zhao, J. Yan, M. Hou, J. Yan, M. Kunz, N. Tamura, H. Zhang, and Z. Yin, *J. Phys. Chem. C* **123**, 17735 (2019).
- ⁷⁸S. Zhai, J. Rojas, N. Ahlberg, K. Lim, M. F. Toney, H. Jin, W. C. Chueh, and A. Majumdar, *Energy Environ. Sci.* **11**, 2172 (2018).
- ⁷⁹Z. Zhang, S. Yang, X. Hu, H. Xu, H. Peng, M. Liu, B. P. Thapaliya, K. Jie, J. Zhao, J. Liu, H. Chen, Y. Leng, X. Lu, J. Fu, P. Zhang, and S. Dai, *Chem. Mater.* **31**, 5529 (2019).
- ⁸⁰M. Balcerzak, K. Kawamura, R. Bobrowski, P. Rutkowski, and T. Brylewski, *J. Electron. Mater.* **48**, 7105 (2019).
- ⁸¹H. Chen, N. Qiu, B. Wu, Z. Yang, S. Sun, and Y. Wang, *RSC Adv.* **9**, 28908 (2019).
- ⁸²M. Biesuz, S. Fu, J. Dong, A. Jiang, D. Ke, Q. Xu, D. Zhu, M. Bortolotti, M. J. Reece, C. Hu, and S. Grasso, *J. Asian Ceram. Soc.* **7**, 127 (2019).
- ⁸³R. K. Patel, S. K. Ojha, S. Kumar, A. Saha, P. Mandal, J. W. Freeland, and S. Middey, *Appl. Phys. Lett.* **116**, 071601 (2020).
- ⁸⁴S. Zhou, Y. Pu, Q. Zhang, R. Shi, X. Guo, W. Wang, J. Ji, T. Wei, and T. Ouyang, *Ceram. Int.* **46**, 7430 (2020).
- ⁸⁵Y. Pu, Q. Zhang, R. Li, M. Chen, X. Du, and S. Zhou, *Appl. Phys. Lett.* **115**, 223901 (2019).
- ⁸⁶J. Gild, M. Samiee, J. L. Braun, T. Harrington, H. Vega, P. E. Hopkins, K. Vecchio, and J. Luo, *J. Eur. Ceram. Soc.* **38**, 3578 (2018).

- ⁸⁷V. I. Sachkov, R. A. Nefedov, and I. V. Amelichkin, *IOP Conf. Ser.: Mater. Sci. Eng.* **597**, 012005 (2019).
- ⁸⁸M. Anandkumar, S. Bhattacharya, and A. S. Deshpande, *RSC Adv.* **9**, 26825 (2019).
- ⁸⁹B. Cheng, H. Lou, A. Sarkar, Z. Zeng, F. Zhang, X. Chen, L. Tan, V. Prakapenka, E. Greenberg, J. Wen, R. Djenadic, H. Hahn, and Q. Zeng, *Commun. Chem.* **2**, 114 (2019).
- ⁹⁰A. Mao, F. Quan, H.-Z. Xiang, Z.-G. Zhang, K. Kuramoto, and A.-L. Xia, *J. Mol. Struct.* **1194**, 11 (2019).
- ⁹¹M. Stygar, J. Dąbrowa, M. Możdziej, M. Zajusz, W. Skubida, K. Mroczka, K. Berent, K. Świerczek, and M. Danielewski, *J. Eur. Ceram. Soc.* **40**, 1644 (2020).
- ⁹²D. Wang, Z. Liu, S. Du, Y. Zhang, H. Li, Z. Xiao, W. Chen, R. Chen, Y. Wang, Y. Zou, and S. Wang, *J. Mater. Chem. A* **7**, 24211 (2019).
- ⁹³A. Radoń, Ł. Hawełek, D. Łukowiec, J. Kubacki, and P. Włodarczyk, *Sci. Rep.* **9**, 20078 (2019).
- ⁹⁴Z. Teng, L. Zhu, Y. Tan, S. Zeng, Y. Xia, Y. Wang, and H. Zhang, *J. Eur. Ceram. Soc.* **40**, 1639 (2020).
- ⁹⁵K. Zhang, W. Li, J. Zeng, T. Deng, B. Luo, H. Zhang, and X. Huang, *J. Alloys Compd.* **817**, 153328 (2020).
- ⁹⁶Z. Lei, X. Liu, R. Li, H. Wang, Y. Wu, and Z. Lu, *Scr. Mater.* **146**, 340 (2018).
- ⁹⁷Y. Dong, K. Ren, Y. Lu, Q. Wang, J. Liu, and Y. Wang, *J. Eur. Ceram. Soc.* **39**, 2574 (2019).
- ⁹⁸J. Zhang, X. Zhang, Y. Li, Q. Du, X. Liu, and X. Qi, *Mater. Lett.* **244**, 167 (2019).
- ⁹⁹D. A. Vinnik, E. A. Trofimov, V. E. Zhivulin, O. V. Zaitseva, S. A. Gudkova, A. Y. Starikov, D. A. Zhrebtsov, A. A. Kirsanova, M. Häßner, and R. Niewa, *Ceram. Int.* **45**, 12942 (2019).
- ¹⁰⁰D. A. Vinnik, E. A. Trofimov, V. E. Zhivulin, O. V. Zaitseva, D. A. Zhrebtsov, A. Y. Starikov, D. P. Sherstyuk, S. A. Gudkova, and S. V. Taskaev, *Ceram. Int.* **46**, 9656 (2020).
- ¹⁰¹A. Kirnbauer, C. Spadt, C. M. Koller, S. Kolozsvári, and P. H. Mayrhofer, *Vacuum* **168**, 108850 (2019).
- ¹⁰²C.-H. Tsau, Z.-Y. Hwang, and S.-K. Chen, *Adv. Mater. Sci. Eng.* **2015**, 353140.
- ¹⁰³M. S. Lal and R. Sundara, *ACS Appl. Mater. Interfaces* **11**, 30846 (2019).
- ¹⁰⁴Y. Zhong, H. Sabarou, X. Yan, M. Yang, M. C. Gao, X. Liu, and R. D. Sisson, *Mater. Des.* **182**, 108060 (2019).